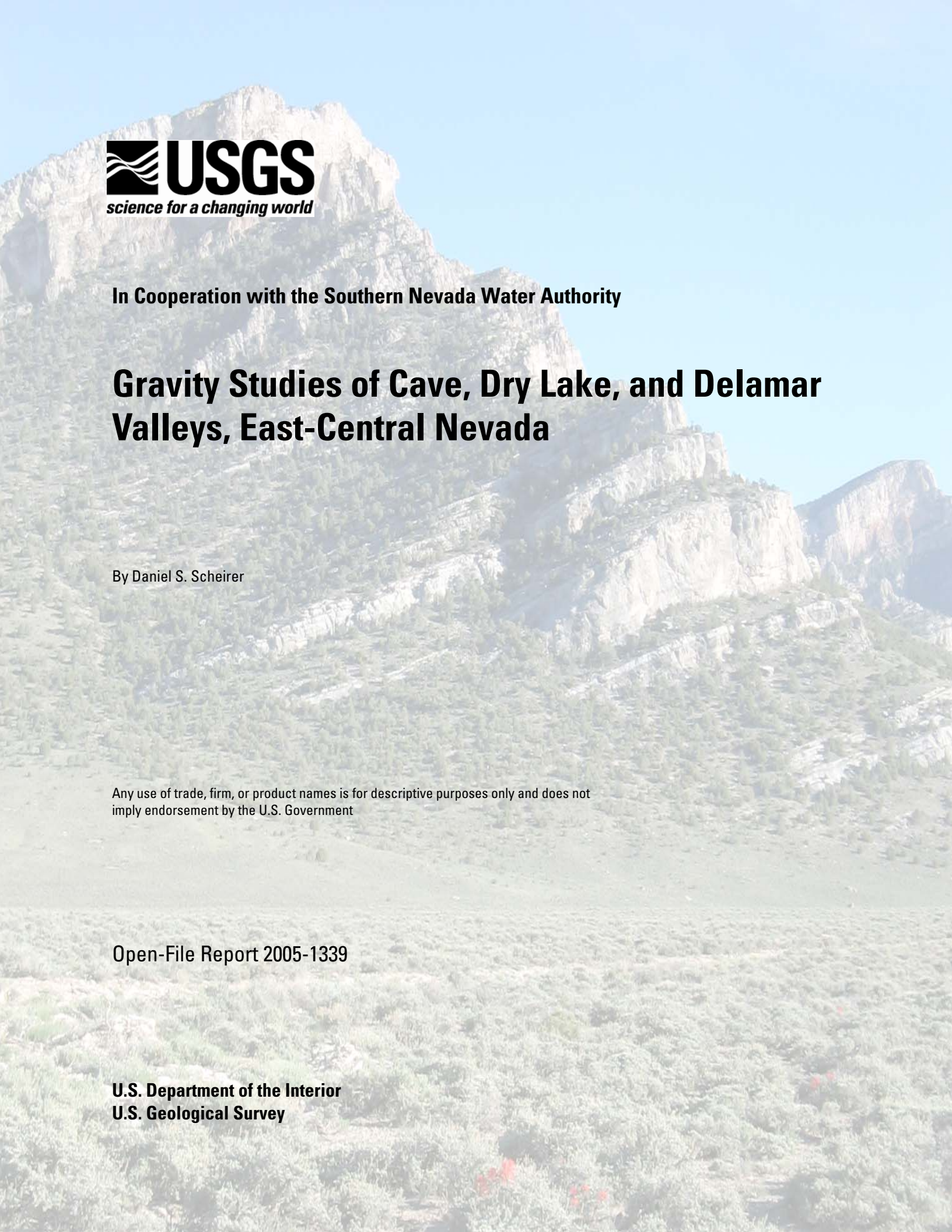

USGS
science for a changing world

In Cooperation with the Southern Nevada Water Authority

Gravity Studies of Cave, Dry Lake, and Delamar Valleys, East-Central Nevada

By Daniel S. Scheirer

Open-File Report 2005-1339

U.S. Department of the Interior
U.S. Geological Survey

Contents

Figures

Tables

Gravity Studies of Cave, Dry Lake, and Delamar Valleys, East-Central Nevada

By Daniel S. Scheirer

Abstract

Analysis of gravity anomalies in Cave, Dry Lake, and Delamar valleys in east-central Nevada defines the overall shape of their basins, provides estimates of the depth to pre-Cenozoic basement rocks, and identifies buried faults beneath the sedimentary cover. In all cases, the basins are asymmetric in their cross section and in their placement beneath the valley, reflecting the extensional tectonism that initiated during Miocene time in this area. Absolute values of basin depths are estimated using a density-depth profile calibrated by deep oil and gas wells that encountered basement rocks in Cave Valley. The basin beneath southern Cave Valley extends down to ~6.0 km, that of Dry Lake Valley extends to ~8.2 km, and that of Delamar Valley extends to ~6.4 km. The ranges surrounding Dry Lake and Delamar valleys are dominated by volcanic units that may produce lower-density basin infill, which in turn, would make the maximum depth estimates somewhat less. Dry Lake Valley is characterized by a slot-like graben in its center, whereas the deep portions of Cave and Delamar valleys are more bowl-shaped. Significant portions of the basins are shallow (<1 km deep), as are the transitions between each of these valleys. A seismic reflection image across southern Cave and Muleshoe valleys confirms the basin shapes inferred from gravity analysis. The architecture of these basins inferred from gravity will aid in interpreting the hydrogeologic framework of Cave, Dry Lake, and Delamar valleys by placing estimates on the volume and connectivity of potential unconsolidated alluvial aquifers and by identifying faults buried beneath basin deposits.

Introduction

In the southern half of Nevada, ground water is organized into a number of extensive regional flow systems (e.g., Harrill and Prudic, 1998) where ground water can flow between adjacent topographic ranges and basins. Subsurface flow occurs within permeable units or along permeable geologic structures. In east-central Nevada, the main flow system is the White River regional ground water flow system (e.g. Eakin, 1966), or alternatively termed the Colorado regional flow system (Harrill and Prudic, 1998). Aquifer units include widely distributed Paleozoic carbonate rocks, locally significant Tertiary volcanic rocks, and Cenozoic basin-fill deposits (cf., Plume and Carlton, 1988, Dettinger and others, 1995, and Harrill and Prudic, 1998). Regional aquifer recharge in the White River flow system occurs by precipitation in primarily the northern mountainous areas with the primary discharge occurring at Muddy River Springs, which form the Muddy River (Dettinger and others, 1995; Page and others, in press).

The valleys that are the focus of this study: Cave, Dry Lake, and Delamar, are situated near the center of the White River regional ground-water flow system, in Lincoln and White Pine counties (Figure 1). Precambrian crystalline basement does not crop out in this area, but is thought to form a deep barrier to ground water transport (D'Agnese and others, 1997). The ranges surrounding the study basins primarily consist of Paleozoic marine rocks, predominantly carbonate units but also minor shale, conglomerate, and quartzite rocks that formed on the western continental margin of North America, and of Tertiary volcanic rocks, Figure 1b (e.g., Tschanz and Pampeyan, 1970; Stewart, 1980). Marine deposition was nearly continuous in this area throughout the Paleozoic, and deposition ceased until continental volcanism, minor intrusion and plutonism, and associated sedimentation occurred during Oligocene and Miocene times. The Caliente caldera complex, in the southern portion of the study area, forms a thick and variable sequence of volcanics that comprise some of the ranges in the south (Figure 1b).

Tectonism initiated in the study area in Miocene time and deformed the Paleozoic units and older volcanics via extensional block-faulting and subsidiary faulting, leading to the present-day basin and range landscape. Erosion of the ranges filled adjacent valleys with alluvial sequences that are unconsolidated or poorly consolidated, and basin-fill occupies about 50% of the exposure within the study area (Figure 1b). In the study area, the geological structures defining the northern ranges, Egan and Schell Creek, are simpler than their counterparts to the south. In the north, the units comprising the ranges dip primarily to the east with steep, range-front normal faults marking their western margins; in the south, the ranges are built of a combination of Paleozoic marine rocks and variably-thick Tertiary volcanic rocks, and they are disrupted by complex arrays of faults related both to the regional extension and to stresses from volcanic processes (Tschanz and Pampeyan, 1970).

The U.S. Geological Survey conducted gravity experiments along Cave, Dry Lake, and Delamar valleys (Figure 1) to help delineate the subsurface configuration of the valleys and to identify faults that may lie beneath alluvial cover. Because of the substantial density contrast between unconsolidated sediments and older marine sedimentary rocks, gravity is a useful tool for this goal.

Gravity Observations and Analysis

In 2003 and 2004, the U.S. Geological Survey collected gravity observations at 468 new sites (Appendix Table A1) to supplement the prior compilation of ~3500 stations in this area (Snyder and others, 1981; Bol and others, 1983; Snyder and others, 1984; Ponce, 1992, 1997). For the recent fieldwork, we established local gravity base stations at the Lanes Ranch Motel, Lund, Nev., at the Hot Springs Motel, Caliente, Nev., and at the Union Pacific Train Station, Caliente, Nev. (Table 1). Values of gravity at these local bases were tied to the IGSN71 gravity datum (Morelli, 1974) via double-loop surveying to the ELYA benchmark at the Ely (Nev.) Airport. New data were collected with a LaCoste-Romberg gravity meter, and station positions were recorded with a Trimble GeoXT Global Positioning System (GPS) receiver. By using fixed GPS reference stations within ~100 km of the gravity observations, latitude and longitude values were calculated via post-processing to have a precision generally better than 1 meter, and elevations had precisions of about 1 meter. At gravity stations situated on outcrop, we collected 153 rock hand-samples at 152 of the stations (Appendix Table A2), and we measured their density and magnetic susceptibility properties in the lab (Johnson and Olhoeft, 1984).

Values of observed gravity were calculated at the new stations by accounting for fluctuations related to tidal accelerations and for instrument drift constrained at the beginning and end of each field day. New gravity stations were collected within coverage gaps of the prior data, especially in the ranges adjacent to the study basins. We used a helicopter to collect many of the stations in rugged terrain (138 sites). Characterizing the gravity variations within the ranges is required to allow accurate separation of the observed gravity anomalies into pre-Cenozoic and Cenozoic contributions, as described in the depth to basement technique below.

For both the prior and new gravity stations, we compared measured station elevations to corresponding elevations of the 10 m (and 30 m in a few areas where higher resolution was unavailable) digital elevation models (DEMs). Where the station elevations differed by 80 feet (24.4 m) or more from the DEM, the gravity station was omitted from further analysis. Where the station elevations differed by a lesser but still significant amount, we inspected those cases and manually removed some of these stations, as well. We then calculated a series of predictable gravity corrections for all of the stations to account for: the global gravity field, the reduction in gravity with increasing elevation (free-air correction), the effect of mass between the station and the geoid (simple Bouguer correction), the effect of topographic variation near the station (terrain correction), and the effect of compensating mass near the base of the crust (isostatic correction). The final gravity anomaly after application of these corrections is termed the isostatic gravity anomaly and is useful for interpretation because it primarily reflects the density variations in the upper- and mid-crust (Simpson and others, 1986). For new gravity stations, estimates were made of the field terrain correction in a zone from the station out to a radius of 68 m; for the prior stations, this innermost terrain correction was not available. For all stations, digital terrain corrections beyond 68 m were calculated from DEMs in two stages: from 68 m to 2 km and from 2 km to 167 km using the algorithm of Plouff (1997). Other parameters that were used in the calculation of gravity corrections are typical for gravity studies in the Basin and Range Province; these include an upper crustal density of 2.67 g/cc, a mantle-crust density contrast of 0.4 g/cc, and a nominal crustal thickness at sea level of 25 km. A typical error of the new gravity stations is estimated to be ~0.2 mGal, and a typical error of the prior gravity stations is thought to be 0.5-1 mGal. In all cases, the errors are

primarily due to elevation and terrain correction uncertainties, and they are small relative to the size of the anomalies that arise from basin structures.

Gravity station data were gridded with a 500 m spacing, which is somewhat finer than the average station-spacing in the valleys (~1 km) and significantly finer that the spacing in the ranges, where gaps up to 4 km exist despite filling in many gaps via helicopter. During the gridding process, we identified a number of prior stations that had gravity values significantly different from their neighbors. To aid in identifying these noise spikes, we upward-continued (e.g., Blakely, 1996) the isostatic gravity field by 500 m, then calculated the difference between the original and upward-continued grids. This difference highlights short-wavelength anomalies in the grid, and individual gravity stations that contributed significant noise were identified and omitted from further analysis. Of the ~3900 gravity stations in the study area, 67 were omitted because their station elevations differed significantly from the DEM values, and 9 of the remaining stations were omitted because of gravity noise spikes. All of the stations collected in 2003 and 2004 passed the noise-editing tests.

Gridded isostatic gravity anomaly data were used to guide the gravity analysis in two modes: to detect significant lateral density interfaces in the subsurface using a maximum horizontal gradient technique (Blakely and Simpson, 1986) and to create models of the depth to pre-Cenozoic basement using the anomaly separation technique of Jachens and Moring (1990). Maximum horizontal gradients of gravity fields are situated above vertical or near-vertical density boundaries in the subsurface, especially for shallow sources. The positions of local maxima of the gravity gradient can help delineate lithologic contacts at depth, especially those related to faults juxtaposing low-density basin fill against consolidated rock. The magnitude of the gradient is a function of the depth to the density boundary and the size of the density contrast, and in practice, the presence of noise in the gravity grid may lead to false identifications of geological boundaries using this technique. The interpretive power of this method is best where maximum gradients are spatially identified in clusters or lineaments.

The depth-to-basement technique endeavors (1) to separate contributions to the isostatic gravity anomaly that arise from Cenozoic sedimentary and volcanic deposits and those from pre-Cenozoic rocks and (2) to convert the low-density contributions from the young deposits into a model of basin depth (Jachens and Moring, 1990). This is an inverse geophysical approach because it calculates model geometry from observations of gravity, constrained by outcrop patterns and with *a priori* assumptions about the density contrast of basin fill relative to surrounding rocks. This method is iterative and has been successfully applied to the entire Basin and Range Province (Saltus and Jachens, 1995) and to individual basins and groups of basins in southern Nevada (e.g., Langenheim and others, 2000). The depth-to-basement method first separates those gravity stations that lie on Cenozoic deposits (termed “basin”) vs. those that lie on pre-Cenozoic rocks; these older units are termed “basement” in this description, a usage that differs from the common description of old, crystalline rocks as basement in many areas. The isostatic gravity anomalies at basement stations are then interpolated across the intervening basins, and differences between the interpolated basement gravity values and those measured at basin stations are attributed to the low-density basin infill. Using a 1-D approximation, the depth of the basin fill is estimated from the size of the basin gravity anomaly at each grid point, and then the gravitational attraction of these interpreted basins is calculated. Where a basement gravity station lies close to basin material, some of the attraction of the low-density infill will influence its gravity value; thus, the calculated basin attraction must removed from the gravity value at each basement station. This process yields estimates of basement gravity, basin gravity, and depth to basement beneath the basins. This sequence is then repeated for multiple iterations until the estimates of basin depth converge. In this study, gravity stations are separated based on their placement on three geological units: pre-Cenozoic basement, Cenozoic sedimentary fill, and Cenozoic volcanic deposits. The depth of the resulting basement surface is assumed to be the thickness of sedimentary deposits where sediments are at the surface and to be the thickness of volcanic deposits where volcanics crop out, although it is likely that sediments overly volcanic deposits in some areas.

A critical input to the depth-to-basement method is the depth variation of the density contrast of the basin fill material relative to the surrounding rock; this density profile is the link to convert basin gravity anomalies to basin depth estimates. Measured density-depth functions are available from deep boreholes in other parts of the Basin and Range Province (e.g. Healey and others, 1984) but not from the study area. We first utilized the density-depth functions used in Jachens and Moring (1990) that were deemed appropriate for the entire Basin and Range Province (Table 2). After some experimentation, discussed below, we adopted density-depth relationships (Table 2) with smaller density contrasts, leading to deeper estimated basins that matched better independent constraints on basement depths. In these density-depth functions, density increases with depth, especially within the uppermost 600 m. Near the surface, sedimentary deposits are less dense than the volcanics; deeper than 600 m, the density-

depth functions are identical. This relationship demonstrates why it is very difficult to separate the geophysical effects of sedimentary and volcanic deposits using gravity methods.

Measured depths to the base of Cenozoic deposits can be used as important constraints to the depth-to-basement estimation. These measurements are available typically from deep boreholes associated with oil and gas exploration (Table 3 indicates those available in Cave and Dry Lake valleys, Hess, 2004), and even if a borehole does not penetrate the entire basin deposit, its bottom depth may be used as a minimum constraint on the depth-to-basement solution. In this area, four deep wells from the MX project (Bunch and Harrill, 1984) are also available for comparison with gravity models (Table 3). Independent basement depth constraints may be applied to the modeling using two approaches: either as *a priori* exact and minimum depth constraints that must be satisfied as the depth-to-basement algorithm iterates, or as post-modeling validation of the depth-to-basement solution. Deciding on which approach to use depends on the distribution of depth constraints and on the availability of measured density-depth functions in the study area. The latter post-modeling approach is utilized in this study for two reasons: deep borehole constraints are sparse, and systematic differences in measured basin depths (from boreholes) and estimated depths (from gravity analysis) will allow testing and modification of the assumed density-depth function. As noted above and described below, we modified the density-depth function of Jachens and Moring (1990) to match borehole depths in Cave Valley more closely.

Rock property measurements are summarized in Table 4 as averages grouped by rock type. While physical properties of individual hand-samples may not represent well the bulk properties of in situ volumes of rock, especially those at depth, the measurements can aid in establishing the density variations among the units. The most common rock types sampled, carbonate and felsic volcanic rocks, have statistically distinct average densities of 2.70 g/cm^3 and 2.34 g/cm^3, respectively. The Paleozoic rock samples, as a whole, average to a density value very close to the 2.67 g/cm^3 assumed for the Bouguer and isostatic gravity corrections. The young volcanic rocks are less dense and more porous (2-10%) than the older sedimentary rocks (<3% porosity). The volcanic rocks are also the only samples to have significantly non-zero magnetic susceptibility.

Results

The results of the gravity analysis are presented as a series of maps in Figure 2 for Cave and northernmost Dry Lake valleys (including Muleshoe Valley) and in Figure 3 for Dry Lake and Delamar valleys.

Cave Valley is bounded by the sinuous Egan and Schell Creek ranges and is segmented into northern and southern halves by the Shingle Pass Fault that bends the southern Egan Range towards the northeast and across much of the oval-shaped valley floor (Figure 2b, Tschanz and Pampeyan, 1970). These ranges are primarily eastward-dipping tilt-blocks with steep normal faults defining their western margins. Smaller faults cross the ranges, segment the ranges into distinct sections, and create topographic passes. Volcanic units are present in a number of areas surrounding Cave Valley but not with significant thickness (Tschanz and Pampeyan, 1970). The southern portion of Cave Valley has a playa and is much flatter than the floor of the northern valley, which is dissected by streams and is marked by a handful of isolated outcrops (Figure 2b).

For Cave Valley, the prior gravity station distribution was adequate for much of the valley area, but there were large gaps in the surrounding Egan and Schell Creek ranges that were filled using helicopter access (Figure 2a). Many of the gaps that remain within the ranges were investigated by air but deemed unsafe as landing sites. Numerous stations in the valley floors were collected to fill existing gaps, to survey along the ECN-01 seismic line, and to collect gravity observations at well sites that provide independent information on depth to the base of valley-fill deposits. In Cave Valley proper, there are 8 oil and gas wells that penetrated basement, and 1 MX well that encountered basement (Figure 2a and Table 3).

The isostatic gravity anomaly of Cave and Muleshoe valleys is characterized by 20-30 mGal lows centered on the valleys relative to the isostatic values in the surrounding ranges. There are significant gravity fluctuations within the ranges, reflecting the lithologic variation within them; for example, the low-relief range along the southeastern margin of Muleshoe Valley is comprised of volcanic rocks and has a relative gravity low (Figures 2b, 2c). The maximum horizontal gradients of the isostatic anomaly over areas with surface sediments are displayed as pink symbols on the isostatic gravity map (Figure 2c). Larger and more continuous maximum gradient picks are present in southern Cave Valley relative to northern Cave Valley. In the south, two main lines of maximum

gradients are found paralleling the eastern and western margins of the valley, with the western group close to the axis of the valley and the eastern group close to the front of the Schell Creek Range. Muleshoe Valley is also lined by steep isostatic gravity gradients along its eastern and western margins, and is marked by diffuse and small gradients on its southern margin where it crosses a small rise that leads into northernmost Dry Lake Valley (Figure 2a, 2c).

The depth-to-basement algorithm separates the isostatic gravity anomaly into portions that arise from the Cenozoic deposits ("basin-fill") vs. those from the pre-Cenozoic rocks ("basement"), and the resulting basin gravity anomaly is illustrated in Figure 2d. The basin gravity anomaly is zero or slightly negative for areas of pre-Cenozoic outcrop, and it achieves the most negative values towards the centers of basins. This anomaly is transformed, via the assumed density-depth function, into a basement depth map, Figure 2e. Basin depths estimated from gravity extend to ~6.0 km in Cave Valley. Maximum depth estimates from the adjacent valleys to the west (White River) and to the east (Lake) are greater, but the gravity coverage is not complete in these areas and careful calibration with independent basement depth constraints has not been performed. In northern Cave Valley, typical basement depths are hundreds of meters, and no site has an estimated depth greater than 1 km. Isolated outcrops extending to the northeast of the Shingle Pass Fault are surrounded by sediments no thicker than 100 m, based on this gravity analysis (Figure 2e). In southern Cave Valley, the basin has depth-to-basement estimates >1 km for more than half of its length; its deepest inferred depth is just east of the valley's axis. The borehole picks to the base of the alluvium are superimposed on the depth-to-basement map (Figure 2e) and show broad agreement in map-view. For comparison, the depth-to-basement map for this area from Saltus and Jachens (1995) is illustrated in Figure 2f. The most striking difference between these two solutions is the 4-fold (500 m vs. 2000 m) resolution increase of the new analysis and its attendant ability to characterize better the geological structures, such as range-front faults, in the study valleys. In addition, the depths of the new estimates are nearly 50% deeper because of the improved density-depth functions (Table 2).

The results of comparisons between the base of alluvium picks from oil and gas wells (Hess, 2004) and MX wells (Table 3) and the depth-to-basement values from the gravity inversion are illustrated in Figure 4. Over the 0 to 2000 m depth range of basement identifications from wells, the estimated basement depths from gravity are centered about the 1:1 equivalence line. Using the greater density-contrast profiles of Jachens and Moring (1990) yielded results where the deeper wells significantly and systematically underestimated the measured basement depths. The match between measured and estimated basement depths is not perfect, and this might stem from a number of reasons: the downhole basement identification might be in error, the identification for a single borehole might not be representative of the true interface at depth averaged over the lateral dimension that contributes to the gravity anomaly measured at the earth's surface, errors in observed or reduced gravity will translate into errors in inferred depth, and densities in the basin deposits likely vary from place to place. While there is some scatter, the overall consistency between the basement depth estimates in this study indicate that the overall form of the depth-to-basement inversions are as correct as can be achieved with the available subsurface observations. It is important to note that observed borehole depths in Cave Valley extend to at most 1900 m, so we cannot test the density-contrast function values between that depth and depths more than twice as great. The two minimum depth constraints, gray circles in Figure 4, should fall to above the 1:1 equivalence line; these wells are located in Dry Lake and Delamar valleys and are discussed below.

An additional view into the subsurface structure of southern Cave Valley and Muleshoe valley is provided by a portion of the industry-shot ECN-01 seismic reflection line (Figure 5). The seismic line crosses near the maximum depth position of Cave Valley (Figure 2e). The seismic reflection image illustrates the asymmetric character of Cave Valley cross section, with a steeper eastern side where the range-front fault of the Schell Creek Range lies and a less-steep western floor leading up to the dip-slope of the Egan Range (Figure 5a). Strong reflectors mark the base of Cave Valley, and a discordant and more horizontal packet of reflectors characterizes much of the deeper valley fill. Weaker subhorizontal reflectors are present in the upper valley fill. The reflectors in the shallow portions of Muleshoe Valley are weak or absent, but in its deeper section exhibit characteristics similar to those of the Cave Valley reflectors. These seismic data are displayed in travel-time, so a quantitative appraisal of seismic depths to basement is not possible. Nevertheless, the inferred basin structure from gravity analysis (Figure 5b) shares a number of similarities with the seismic image: Cave Valley is asymmetric and reminiscent of a half-graben and the overall shapes of Cave vs. Muleshoe, in deeper portions, look similar between the seismic and gravity models. American Petroleum Institute (API) well 27-017-05221 is superimposed schematically on Figure 5b to illustrate its general agreement with the gravity depth-to-basement estimate and to show its position with respect to the seismic structures.

Dry Lake Valley is bounded by the North Pahroc Range in the west and the Highland and Bristol ranges in the east, and the valley is marked by low saddles to the north and south. The surrounding ranges are intensely faulted and are comprised more of volcanic units than are the ranges surrounding Cave Valley (Tschanz and Pampeyan, 1970). Stations were added throughout the valley and adjacent ranges (Figure 3a). The isostatic gravity anomaly has a >30 mGal negative value in the center of the valley; large maximum horizontal gradients mark an area slightly displaced to the east of the valley axis, and smaller gradients delineate the ends of the basin (Figure 3c). The basin gravity anomaly (Figure 3d) emphasizes the narrowness of the central basin gravity anomaly, which has an aspect ratio of ~5 and a magnitude ~10 mGal greater than the anomaly in Cave Valley.

The depth-to-basement solution for Dry Lake Valley exhibits a narrow slot-like depression along most of the valley that is slightly displaced to the east of the valley's centerline. Away from the slot, basin depths are generally <1 km, and within the slot most depths are >3 km and some are as deep as 8 km. No deep oil and gas or MX wells provide independent measures of basin depth in Dry Lake Valley, so the accuracy of the gravity to depth conversion depends on the appropriateness of the assumed density-depth function utilized in this study (Table 2) that was constrained in Cave Valley. Because the ranges surrounding Dry Lake Valley are composed predominantly of Tertiary volcanics, the sedimentary infill might have lower density than in Cave Valley, in which case the density contrasts with bedrock would be larger and the inverted basin depths would be shallower. Using the density-depth function of Jachens and Moring (1990), Dry Lake Valley would have a maximum basin depth of 6 km. Notwithstanding the question of the magnitude of the basin floor topography, the shape of the basin slot, with relatively flat shelves leading to the adjacent ranges, is robust and independent of any particular density-depth assumptions. No seismic lines are available across Dry Lake Valley, so models of the basin geometry depend on the analysis and interpretation of gravity data alone.

Delamar Valley (Figure 3) is surrounded by volcanic ranges to the west, south, and east that are highly faulted. The isostatic gravity anomaly is similar to those in the other valleys in the study area, but the maximum horizontal gradients are only sporadically clustered along some sections of the South Pahroc (to the west) and Delamar (to the east) ranges. These ranges have lower isostatic gravity anomalies relative to ranges comprised of older, non-volcanic rocks, illustrating their low average densities (Figure 3c), despite the presence of shallow and dense Proterozoic rocks at the Delamar mining district to the east of the valley. The basin gravity anomaly (Figure 3d) has a minimum restricted to the southern half of Delamar Valley, which leads to the bowl-shaped basin inferred from the gravity inversion (Figure 3e). The maximum depth is almost 6.5 km, and it is located west of the center of the southern portion of Delamar Valley. Elsewhere, much of the valley has depths of 1-2 km. Again, no exact constraints on basement depth are available from well picks, so the inferred depths are based on calibration at Cave Valley. Like Dry Lake Valley, the volcanic ranges surrounding Delamar Valley likely create lower-density basin infill than in Cave Valley, where the density-depth profile was validated. Assuming the Jachens and Moring (1990) density function that utilizes lower-densities that used in this study, the deepest part of Delamar Valley would be ~4 km below the valley floor.

Discussion

The basin shapes of Cave, Dry Lake, and Delamar valleys are well discerned by gravity analysis, and they have distinct characters. The northern Cave Valley basin is filled by a thin (<1 km) accumulation of sediments that is discontinuous, except for a <100 m layer, with the deeper southern Cave Valley basin. The deeper basin has the form of an elongate bowl, with asymmetric sides that reflect the block faulting of the Egan and Schell Creek ranges. Muleshoe Valley is a shallower basin that is more symmetric than Cave Valley. In Dry Lake Valley, the deep basin is a narrow slot within the interior of the valley and running along most of its length. While the surrounding ranges are highly tectonized, the most significant faults buried beneath the sedimentary deposits are displaced away from the range fronts to form a slot-like graben in Dry Lake Valley. Whether the shoulders to the graben are simply buried, erosional pediment surfaces or whether they are regions between distinct fault systems proximal and distal to the range-fronts is unknown without further geological and geophysical observations. The southern portion of Delamar Valley is bowl-shaped and significantly deeper than the northern half of the valley. A small, ~1-km deep basin-divide between the Delamar and Dry Lake valley basins occurs ~5 km north of the subtle topographic divide between the valleys. One common feature of all of the study basins is that their maximal depths occur where the valley elevations are lowest, indicating a long-term connection between the geologic structures that deepen the

basins and those that govern geomorphology in the study area. In Cave, Dry Lake, and Delamar Valleys, the size and shape of the surface playas are good proxies for the locations of maximal basin depths.

Uncertainty in the density-depth profiles utilized in the depth-to-basement process translates into the greatest uncertainties in magnitude of basin depths. For Cave Valley, the oil and gas wells that penetrate basin infill to depths ~35% of the maximum modeled depths are useful to constrain the density-depth function at shallow levels. Performing velocity analysis and depth migration of the ECN-01 seismic reflection line would add another independent constraint of the deep basin depths across southern Cave Valley, but the accuracy of these depths would depend on the quality of the velocities recovered from the seismic records. In the Dry Lake and Delamar valleys, neither deep borehole nor seismic constraints are available, so the actual basin depths could vary from those shown in this study. If the material filling the southern valleys is dominated by lower density volcanic units than the dominant Paleozoic rocks of Cave Valley, then the basin-fill density contrasts in Dry Lake and Delamar valleys are likely to be greater, which would lead to shallower basement surfaces inferred from gravity analysis in these southern basins. The trade-off between the assumed physical properties of the basin material and the magnitude of the resultant depth solutions is a fundamental limitation of interpreting potential fields, such as gravity.

Analysis of gravity anomaly gradients indicates that buried faults generally bound the deepest portions of basins and that these faults are continuous and steep over much of the length of the basins. There is no clear association of inferred buried faults and those that criss-cross the surrounding ranges, indicating that if the exposed faults continue beneath the basin infill, they do not juxtapose units of significant density contrast nor do they play a major role in defining the gross architecture of the basin.

The basin architecture inferred from gravity analysis will aid in interpreting the hydrogeologic framework of Cave, Dry Lake, and Delamar valleys in a number of ways. First, the depth-to-basement analysis allows estimation of the placement and volumes of basin-fill aquifers and their potential connections between basins. As noted above, most of the basins are asymmetric in shape and position within a valley, and they have only shallow connections from one basin to another. Second, buried valley-parallel faults are continuous along all of the basins, but these occur in different positions with respect to the valley center and range-fronts. The faults within Dry Lake Valley form a slot-like graben that is distinct from the bowl-shaped basins of southern Cave and Delamar valleys. Other geophysical or geological observations are required to assess how continuous these faults are beneath the basin fill, continuity that would have significant implications for ground-water connections in the carbonate aquifer system.

Acknowledgments

We thank the Southern Nevada Water Authority for project funding. We are grateful to Robert Morin, Bruce Chuchel, and Allegra Hosford Scheirer for their assistance in the field, to Jeremy Lui for lab assistance, and to John Miller who processed the ECN-01 seismic data. This study was improved by reviews of Gary Dixon, Thomas Hildenbrand, Edward Mankinen, and David Ponce.

Table 1. Gravity base stations used for data collected in 2003 and 2004.

[Datums: latitude and longitude, NAD27; elevations, NGVD29; gravity values, IGSN71]

Base name	Latitude	Longitude	Elevation (m)	Observed gravity (mGal)	Description
ELYA[1]	39° 17.593'N	114° 50.513'W	1906.0	979,480.08	Ely Airport, Nev.
LUNDLR	38° 54.839'N	115° 02.591'W	1711.2	979,504.86	Lanes Ranch Motel, Lund, Nev.
CALHSM	37° 37.266'N	114° 30.588'W	1343.8	979,516.06	Hot Springs Motel, Caliente, Nev.
CALTRN	37° 36.732'N	114° 30.831'W	1336.2	979,515.51	Union Pacific Stn., Caliente, Nev.

[1]Part of the World Reference Gravity Network (Jablonsky, 1974)

Table 2. Cenozoic density-depth functions.

[Density contrasts are basin infill-density minus surrounding bedrock density]

Depth range (km)	Sedimentary density contrast (g/cm3) (Jachens & Moring, 1990)	Volcanic density contrast (g/cm3) (Jachens & Moring, 1990)	Sedimentary density contrast (g/cm3) (this study)	Volcanic density contrast (g/cm3) (this study)
0-0.2	-0.65	-0.45	-0.60	-0.40
0.2-0.6	-0.55	-0.40	-0.50	-0.35
0.6-1.2	-0.35	-0.35	-0.30	-0.30
>1.2	-0.25	-0.25	-0.20	-0.20

Table 3. Deep borehole basement constraints.

[Datums: latitude and longitude, NAD27; elevations, NGVD29]

Well ID[1]	Valley	Latitude	Longitude	Surface elevation (m)	Total depth (m)	Depth to basement (m)
27-033-05200	Cave	38° 46.70'N	114° 50.21'W	1981	1529	1027
27-017-05210	Cave	38° 31.25'N	114° 48.20'W	1856	1191	366
27-017-05220	Cave	38° 27.61'N	114° 50.91'W	1832	1707	995
27-017-05001	Cave	38° 26.59'N	114° 49.44'W	1840	2141	1891
27-017-05200	Cave	38° 26.11'N	114° 55.59'W	1890	149	4
27-017-05228	Cave	38° 25.67'N	114° 53.10'W	1825	1856	635
27-017-05229	Cave	38° 25.67'N	114° 53.10'W	1822	1621	547
27-017-05221	Cave	38° 22.31'N	114° 50.35'W	1820	2073	1554
27-017-05224	Dry Lake	37° 55.00'N	114° 36.80'W	2012	3535	325
Cave Valley	Cave	38° 28.12'N	114° 52.17'W	1831	141	111
Dry Lake Valley	Dry Lake	38° 05.52'N	114° 53.70'W	1695	730	104
Dry Lake Valley	Dry Lake	37° 42.25'N	114° 45.52'W	1414	398	N/A
Delamar Valley	Delamar	37° 26.65'N	114° 52.15'W	1436	370	N/A

[1]API number for oil and gas wells; valley name for MX wells.

Table 4. Average physical properties of rock samples, grouped by rock type.

[Average property values are followed by 1-standard deviation values in parentheses.]

Rock type	Number of samples	Grain density (g/cm3)	Saturated bulk density (g/cm3)	Dry bulk density (g/cm3)	Porosity (%)	Susceptibility (10-3 SI)
Carbonate	57	2.73 (0.09)	2.70 (0.11)	2.68 (0.13)	1.7 (1.9)	0.0 (0.1)
Sandstone	12	2.59 (0.07)	2.55 (0.10)	2.53 (0.11)	2.4 (2.1)	0.1 (0.2)
Quartzite	6	2.62 (0.03)	2.61 (0.04)	2.60 (0.04)	0.8 (0.4)	0.0 (0.0)
Felsic Volcanic	60	2.46 (0.12)	2.34 (0.17)	2.25 (0.23)	9.7 (8.2)	3.3 (3.7)
Interm. Volcanic	14	2.53 (0.17)	2.50 (0.17)	2.48 (0.17)	2.1 (1.4)	6.4 (5.6)
Mafic Volcanic	3	2.50 (0.21)	2.43 (0.28)	2.37 (0.35)	6.3 (8.6)	5.2 (3.7)
Granite	1	2.51 (N/A)	2.49 (N/A)	2.47 (N/A)	1.4 (N/A)	0.2 (N/A)

Literature Cited

Blakely, R.J., 1996, Potential Theory in Gravity and Magnetic Applications: Cambridge University Press, 441 p.

Blakely, R.J., and Simpson, R.W., 1986, Approximating edges of source bodies from magnetic or gravity anomalies: Geophysics, v. 51, p. 1494-1498.

Bol, A.J., Snyder, D.B., Healey, D.L., and Saltus, R.W., 1983, Principal facts, accuracies, sources, and base station descriptions for 3672 gravity stations in the Lund and Tonopah 1^0 x 2^0 quadrangles, Nevada: available from National Technical Information Service, U.S. Department of Commerce, Springfield, VA 22152, PB81-1780, 86 p.

Bunch, R.L., and Harrill, J.R., 1984, Compilation of selected hydrologic data from the MX missile-siting investigation, east-central Nevada and western Utah: U.S. Geological Survey Open-File Report 84-702, 123 p.

D'Agnese, F.A., Faunt, C.C., Turner, K., and Hill, M.C., 1997, Hydrogeologic evaluation and numerical simulation of Death Valley regional ground-water flow system, Nevada and California: Water Resources Investigations Report 96-4300, 124 p.

Dettinger, M.D., Harrill, J.R., Schmidt, D.L, and Hess, J.W., 1995, Distribution of carbonate-rock aquifers and the potential for their development, southern Nevada and adjacent parts of California, Arizona, and Utah: U.S. Geological Survey Water Resources Investigations Report 91-4146, 100 p.

Eakin, T.E., 1966, A regional interbasin groundwater system in the White River area, southeastern Nevada: Water Resources Research, v. 2, p. 251-271.

Harrill, J.R., and Pruric, D.E., 1998, Aquifer systems in the Great Basin region of Nevada, Utah and adjacent sates – Summary report: U.S. Geological Survey Professional Paper 1409A, 61p.

Healey, D.L, Clutsom, F.G., and Glover, D.A., 1984, Borehole gravity meter surveys in drill holes USW G-3, UE-25p1, and UE-25c1: U.S. Geological Survey Open-File Report 84-672, 16 p.

Hess, R.H., 2004, Nevada oil and gas well database (NVOILWEL), Nevada Bureau of Mines and Geology Open-File Report 04-1, 288 p.

Jablonski, H. M., 1974, World relative gravity reference network North America, Parts 1 and 2: U.S. Defense Mapping Agency Aerospace Center Reference Publication no. 25, originally published 1970, revised 1974, with supplement of IGSN 71 gravity datum values, 1261 p.

Jachens, R.C., and Moring, B.C., 1990, Maps of the thickness of Cenozoic deposits and the isostatic residual gravity over basement for Nevada: U.S. Geological Survey Open-File Report 90-404, 15 p., 2 plates, scale 1:1,000,000.

Johnson, G.R., and Olhoeft, G.R., 1984, Density of rocks and minerals, *in* Carmichael, R.S., ed., CRC Handbook of Physical Properties of Rocks, Vol. 3: Boca Raton, Fla., CRC Press, Inc., p. 1-38.

Langenheim, V.E., Glen, J.M., Jachens, R.C., Dixon, G.L., Katzer, T.C., and Morin, R.L., 2000, Geophysical constraints on the Virgin River depression, Nevada, Utah, and Arizona: U.S. Geological Survey Open-File Report 00-407, 26 p.

Morelli, C., 1974, The International Gravity Standardization Net 1971: International Association of Geodesy Special Publication no. 4, 194 p.

Page, W.R., Dixon, G.L., Rowley, P.D., and Brickey, D.W., in press, Geologic map of the White River flow system and adjacent areas, Nevada, Utah, and Arizona: Nevada Bureau of Mines and Geology Map Series, 1:250,000 scale.

Plouff, D., 1977, Preliminary documentation for a FORTRAN program to computer gravity terrain corrections based on topography digitized on a geographic grid: U.S. Geological Survey Open-File Report 77-535, 45 p.

Plume, R.W., and Carlton, S.M., 1988, Hydrogeology of the Great Basin region of Nevada, Utah, and adjacent states: U.S. Geological Survey Hydrologic Investigations Atlas HA-694-A, scale 1:1,000,000.

Ponce, D.A., 1992, Bouguer gravity map of Nevada – Ely sheet: Nevada Bureau of Mines and Geology Map 99, scale 1:250,000.

Ponce, D.A., 1997, Gravity data of Nevada: U.S. Geological Survey Digital Data Series DDS-42, 27 p, CD-ROM.

Saltus, R.W., and Jachens, R.C., 1995, Gravity and basin-depth maps of the Basin and Range Province, western United States: U.S. Geological Survey Geophysical Investigations Map GP-1012, 15 p., scale 1:2,500,000.

Simpson, R.W., Jachens, R.C., Blakely, R.J., and Saltus, R.W., 1986, A new isostatic residual gravity map of the conterminous United States with a discussion on the significance of isostatic residual anomalies: Journal of Geophysical Research, v. 91, p. 8348-8372.

Snyder, D.B., Wahl, R.R., and Currey, F.E., 1981, Bouguer gravity map of Nevada – Caliente sheet: Nevada Bureau of Mines and Geology Map 70, scale 1:250,000.

Snyder, D.B., Healey, D.L., and Saltus, R.W., 1984, Bouguer gravity map of Nevada – Lund sheet: Nevada Bureau of Mines and Geology Map 80, scale 1:250,000.

Stewart, J.H., 1980, Geology of Nevada: Nevada Bureau of Mines and Geology Special Publication 4, 136 p.

Stewart, J.H., and Carlson, J.E., 1978, Geologic map of Nevada: U.S. Geological Survey, scale 1:500,000.

Tschanz, C.M., and Pampeyan, E.H., 1970, Geology and mineral deposits of Lincoln County, Nevada: Nevada Bureau of Mines and Geology Bulletin 73, 188 p.

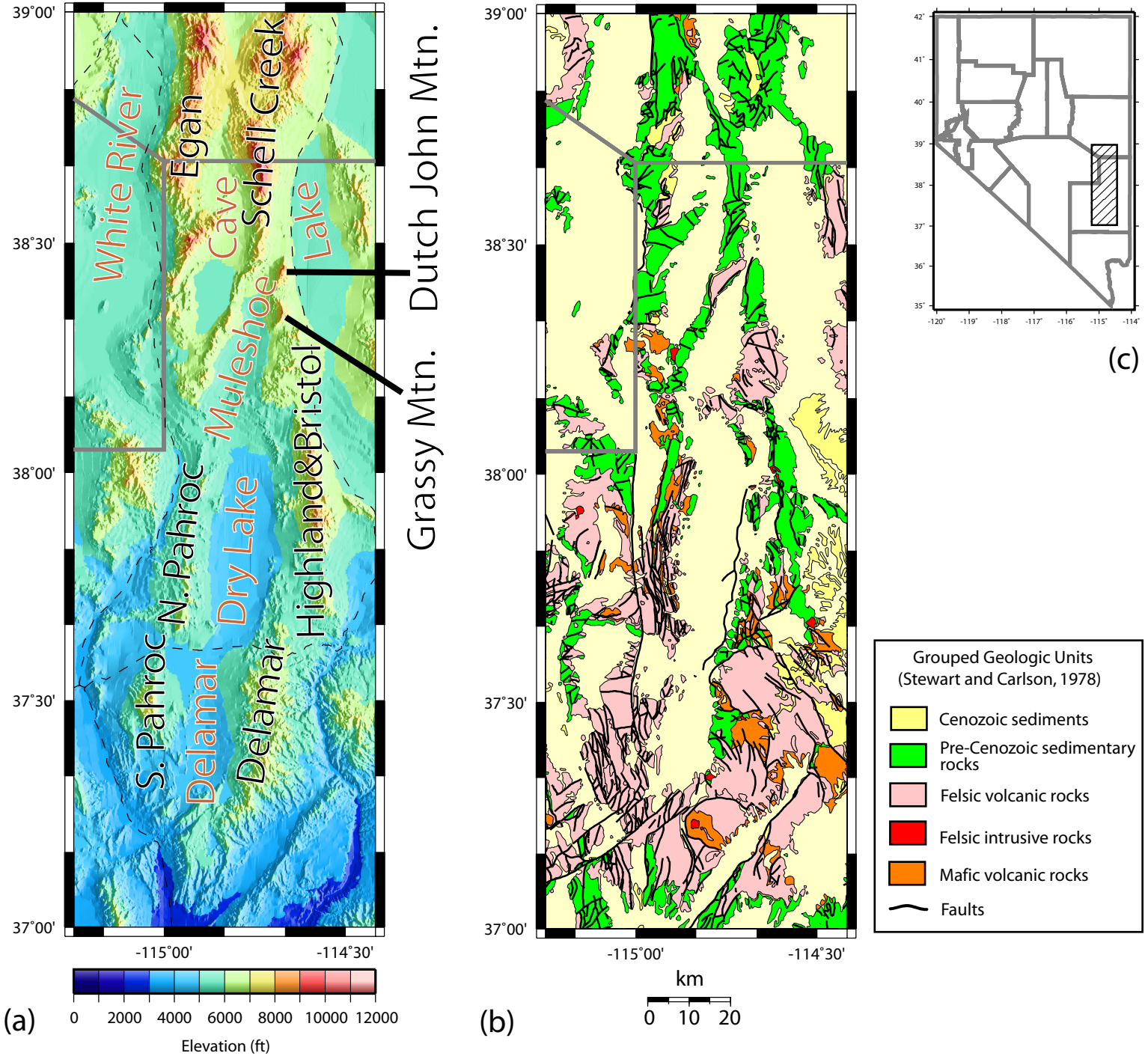

Figure 1. Index map of the study area. 1a) Shaded-relief topography, with labels of the major basins and ranges. Gray lines indicate boundaries of Lincoln, White Pine, and Nye counties in this and subsequent maps. Dashed lines indicate US Highway 93 and Nevada Route 318. 1b) Generalized geology from Stewart and Carlson (1978). 1c) Index map of Nevada showing study area (hachured).

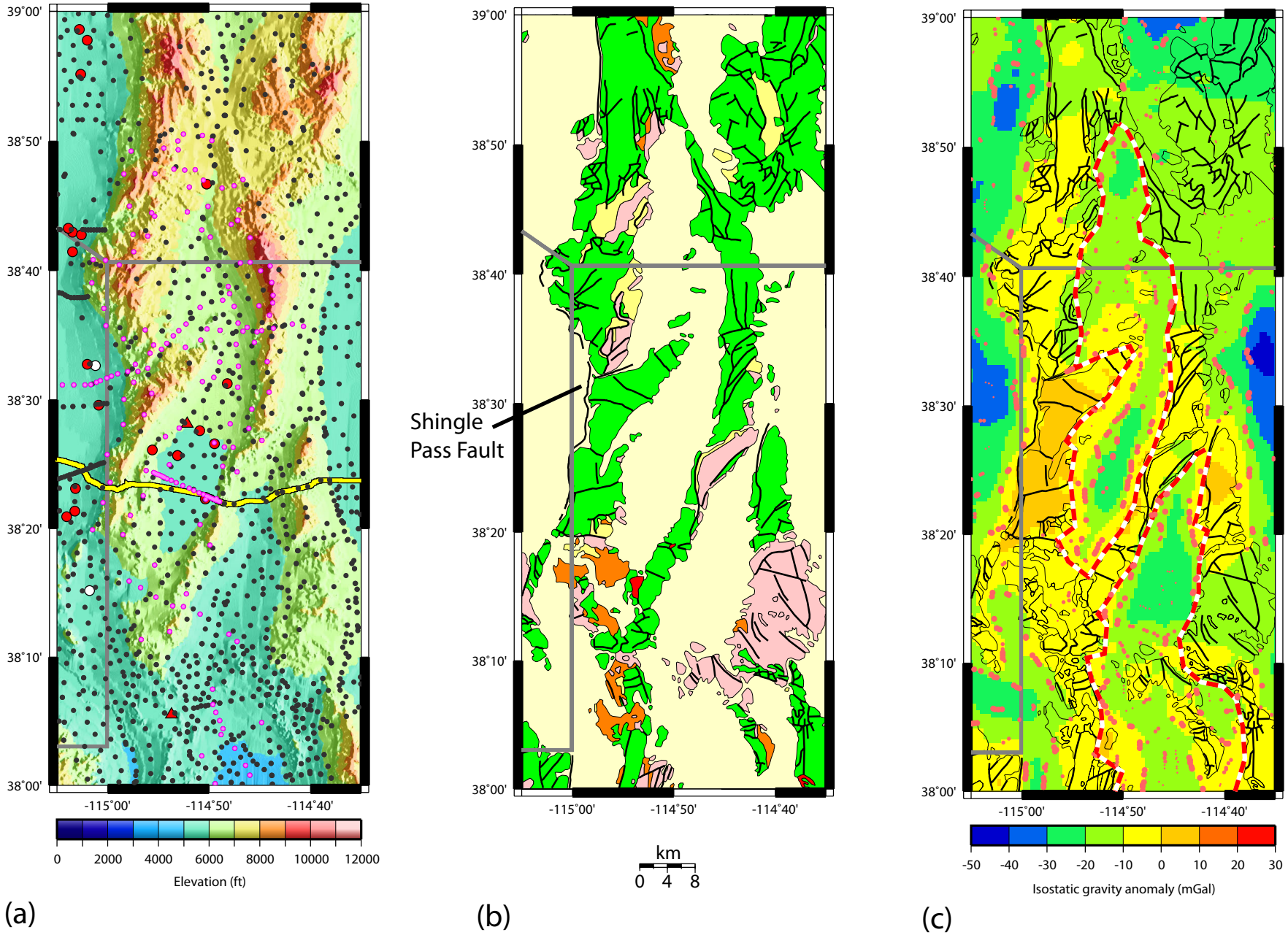

Figure 2 . Cave and Muleshoe valley results. 2a) Shaded -relief topography, with small black circles indicating gravity stations collected prior to 2003 and small magenta circles indicating gravity stations collected by the USGS in 2003 and 2004. Larger circles indicate oil and gas wells; red -fill indicates wells that pass through the entire alluvial section, and white-fill indicates those that bottom in alluvium. Red triangles indicate MX wells that pass t hrough the entire alluvial section. Yellow line indicates the position of the ECN -01 seismic reflection line. 2b) Geology, as in Figure 1b). 2c) Isostatic gravity anomaly map. Red dashed line indicates the outline of the alluvial basins, and thin lines mark the generalized geology of Figure 2b). Pink circles denote the locations of local maxima of the horizontal gradient of the isostatic anomaly field. Only those locations that fall on mapped alluvium are shown, and they are sized according to whether they fall in the lower, middle, or upper thirds of the gradient magnitude distribution.

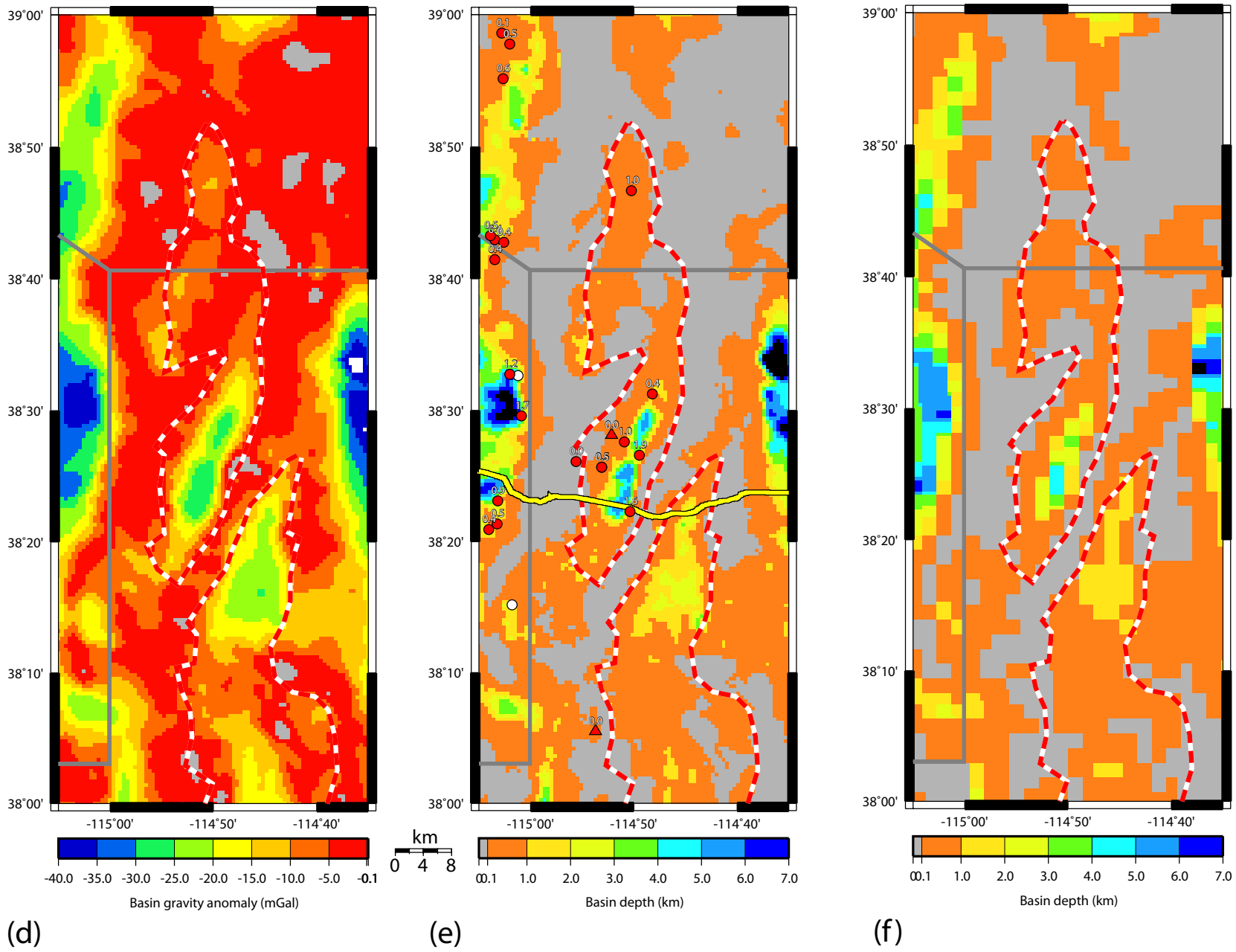

Figure 2 (continued) . 2d) Basin gravity anomaly derived from the depth-to-basement algorithm described in the text. 2e) Calculated basin depth, based on the basin gravity anomaly (2d). Symbols of oil and gas and MX wells are as in (2a), and depths in kilometers to the base of the alluvium are annotated above the symbols. Yellow line indicates the position of the ECN-01 seismic reflection line.

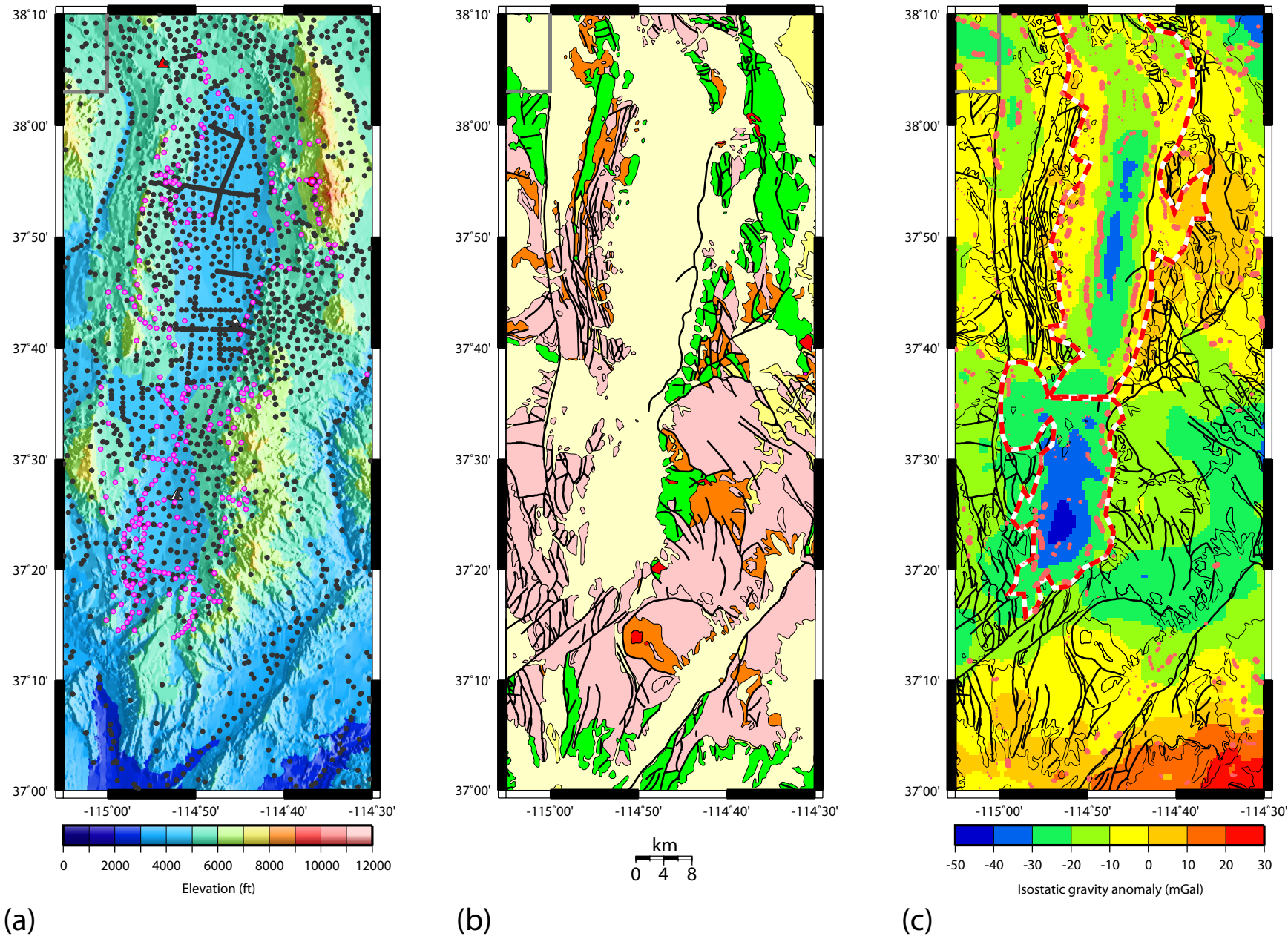

Figure 3. Dry Lake and Delamar valley results. 3a) Shaded-relief topography, with small black circles indicating gravity stations collected prior to 2003 and small magenta circles indicating gravity stations collected by the USGS in 2003 and 2004. Larger circles indicate oil and gas wells; red-fill indicates wells that pass through the entire alluvial section, and white-fill indicates those that bottom in alluvium. Red triangles indicate MX wells that pass through the entire alluvial section, and white triangles indicate MX wells that bottom in alluvium. 3b) Geology, as in Figure 1b). 3c) Isostatic gravity anomaly. Red dashed line indicates the outline of the alluvial basins, and thin lines mark the generalized geology of Figure 3b). Pink circles denote the locations of local maxima of the horizontal gradient of the isostatic anomaly field. Only those locations that fall on mapped alluvium are shown, and they are sized according to whether they fall in the lower, middle, or upper thirds of the gradient magnitude distribution.

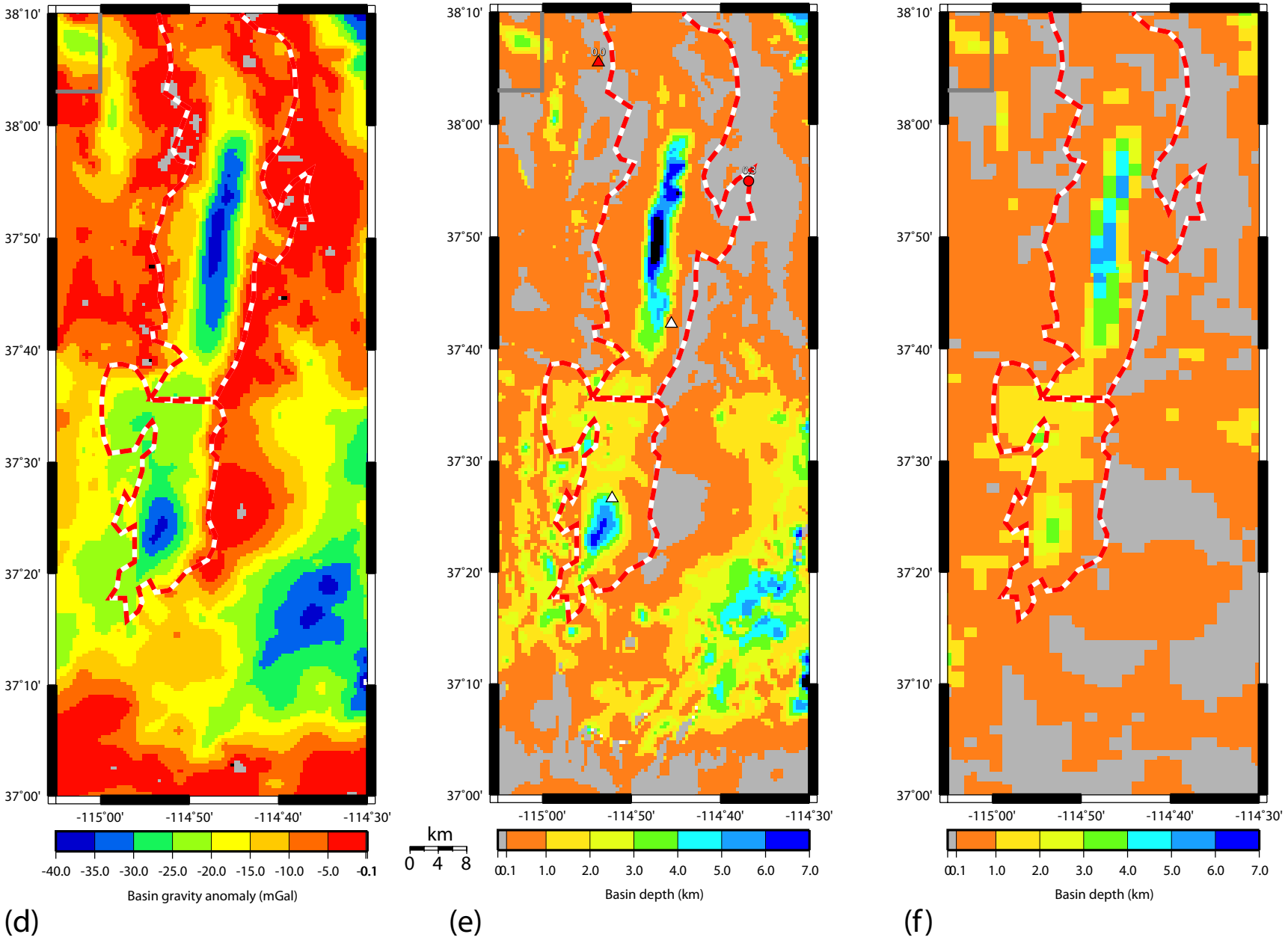

Figure 3 (continued) . 3d) Basin gravity anomaly derived from the depth-to-basement algorithm described in the text. 3e) Calculated basin depth, based on the basin gravity anomaly (3d). Symbols of oil and gas and MX wells are as in (3a), and depths in kilometers to the base of the alluvium are annotated above the symbols. 3f) Calculated basin depth from Saltus and Jachens, 1995.

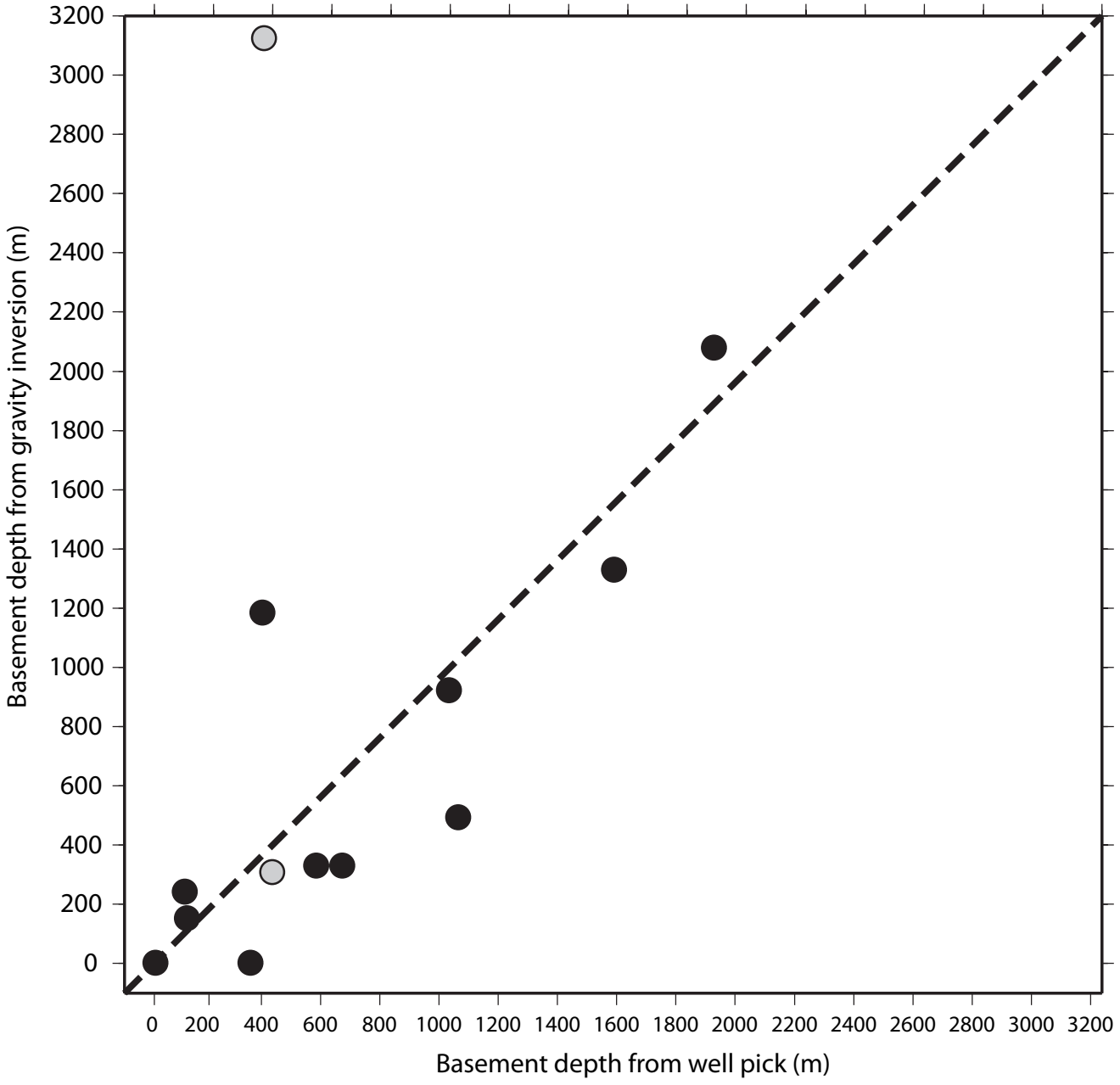

Figure 4. Comparison of basement depths from borehole picks (x-axis) vs. those from gravity depth-to-basement analysis (y-axis). Black circles are wells where exact basement depth constraints were available; gray circles denote wells that bottomed in Cenozoic deposits, and hence their depth is a minimum estimate. Because the black points cluster along the 1:1 dashed line, the density-depth relationship is appropriate for this area.

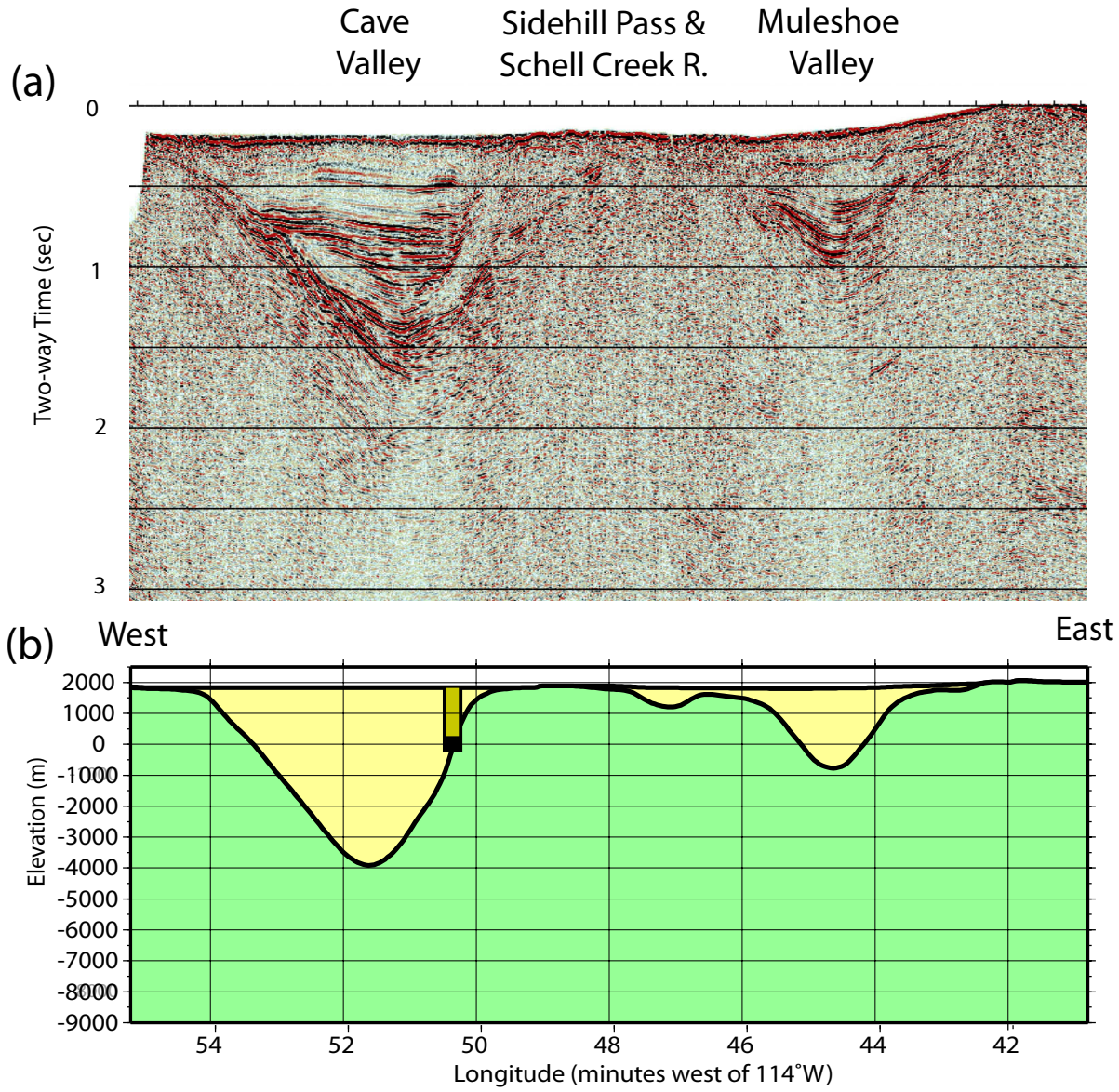

Figure 5. Cross section of southern Cave and northern Muleshoe valleys (cf. Figures 2a, 2e). 5a) ECN-01 seismic reflection section displayed in time. 5b) Results of gravity depth-to-basement inversion with low density basin-fill in yellow; vertical exaggeration = 1.5. API well 27-017-05221 is displayed on the section, and its alluvial interval is shown in dark yellow.

Appendix

Table A1. Principal facts for gravity stations collected in 2003 and 2004 in Cave, Dry Lake, and Delamar Valleys.

[Datums: latitude and longitude, NAD27; elevations, NGVD29. FAA, free-air anomaly; ITC, inner terrain correction calculated out to 2 km; TTC, total terrain correction; CBA, complete Bouguer anomaly, ISO, isostatic anomaly]

Station	Latitude north (deg min)	Longitude west (deg min)	Elevation (feet)	Observed gravity (mGal)	FAA (mGal)	ITC (mGal)	TTC (mGal)	CBA (mGal)	ISO (mGal)
03L001	38 49.24	114 57.67	6433.2	979460.49	0.98	0.60	3.82	-216.13	-11.56
03L002	38 47.48	114 58.40	7647.9	979376.37	33.59	12.90	18.44	-210.30	-7.01
03L003	38 45.00	114 57.83	7407.7	979402.94	41.24	1.97	5.02	-207.88	-5.45
03L004	38 44.47	114 55.65	8214.0	979344.73	59.57	3.15	7.31	-214.71	-12.46
03L005	38 44.21	114 55.36	8140.2	979350.89	59.18	2.53	6.31	-213.60	-11.39
03L006	38 42.68	114 56.04	8211.4	979349.03	66.26	1.10	5.34	-209.91	-8.54
03L007	38 41.46	114 57.42	8312.7	979346.75	75.29	0.63	5.58	-204.09	-3.56
03L008	38 40.44	114 58.85	8503.3	979331.73	79.68	1.26	8.12	-203.63	-3.92
03L009	38 40.79	115 00.20	8185.2	979348.76	66.31	2.72	10.33	-203.98	-4.27
03L010	38 40.84	115 01.43	6976.7	979424.68	28.60	2.31	5.96	-204.90	-4.88
03L011	38 42.80	114 57.50	7397.7	979402.94	43.54	2.11	4.51	-205.76	-4.30
03L012	38 39.06	115 01.56	6564.6	979448.76	16.58	2.46	5.20	-203.62	-4.26
03L013	38 37.08	115 00.37	6477.0	979452.10	14.59	1.72	4.16	-203.66	-5.04
03L014	38 35.75	115 00.16	6143.9	979470.30	3.45	1.55	3.28	-204.31	-6.12
03L015	38 34.74	114 58.42	6324.9	979458.67	10.31	0.97	2.68	-204.23	-6.24
03L016	38 32.76	114 57.27	6730.1	979433.21	25.84	1.77	3.64	-201.57	-4.47
03L017	38 31.37	114 57.42	7712.6	979362.00	48.99	14.28	20.61	-194.94	1.05
03L018	38 33.61	114 55.82	7490.5	979376.78	39.61	5.24	8.16	-209.19	-11.70
03L019	38 34.25	114 55.45	7566.2	979370.60	39.60	3.37	6.25	-213.69	-15.86
03L020	38 35.41	114 56.28	7746.6	979362.68	46.93	1.77	5.46	-213.31	-15.12
03L021	38 30.03	114 58.38	6099.1	979473.50	10.84	1.40	3.98	-194.70	1.10
03L022	38 28.08	114 58.46	5971.6	979478.88	7.10	1.90	4.17	-193.89	0.99
03L023	38 25.76	115 00.03	6018.6	979470.09	6.13	4.60	6.39	-194.24	-0.81
03L024	38 23.60	114 59.75	6290.8	979460.52	25.31	2.22	3.97	-186.78	5.61
03L025	38 22.02	115 00.45	6056.6	979470.91	16.01	3.12	4.52	-187.53	4.02
03L026	38 19.91	115 01.48	5838.9	979482.14	9.88	1.12	1.87	-188.88	1.62
03L027	38 19.53	114 58.48	6933.9	979403.19	34.39	5.16	7.50	-196.11	-5.69
03L028	38 21.04	114 57.73	7312.4	979393.04	57.59	1.39	4.90	-188.42	2.71
03L029	38 22.55	114 56.47	7158.3	979401.56	49.41	2.52	5.30	-190.93	1.19
03L030	38 24.51	114 56.19	7203.6	979398.29	47.53	3.31	6.42	-193.25	-0.13
03L031	38 27.14	114 54.28	6326.3	979456.57	19.50	0.88	2.08	-195.69	-0.62
03L032	38 28.86	114 56.38	8755.2	979299.35	87.98	7.70	21.44	-190.57	3.99
03L033	38 30.50	114 55.63	9782.7	979222.22	104.96	13.66	37.11	-192.80	2.33
03L034	38 37.29	114 45.06	7588.8	979374.58	41.24	4.26	7.89	-211.19	-10.45
03L035	38 40.60	114 46.89	7294.3	979396.21	30.33	0.80	3.91	-216.05	-13.90
03L036	38 40.66	114 45.93	7957.2	979352.84	49.16	3.41	8.00	-215.70	-13.72
03L037	38 42.54	114 45.94	8703.8	979307.26	70.95	3.63	9.47	-217.83	-15.41
03L038	38 43.88	114 47.17	8468.1	979325.29	64.87	2.75	7.42	-217.95	-14.97
03L039	38 44.70	114 47.08	8117.7	979349.24	54.69	1.82	4.80	-218.83	-15.34
03L040	38 49.47	114 54.44	8515.1	979338.38	74.15	1.22	6.21	-211.48	-7.21
03L041	38 47.50	114 55.32	8436.4	979339.63	70.90	1.17	6.02	-212.23	-8.76
03L043	38 47.04	114 46.65	7964.8	979363.82	51.46	0.90	3.02	-218.64	-14.18
03L044	38 43.57	114 47.80	7642.8	979380.32	42.82	1.18	3.36	-215.98	-12.86
03L045	38 40.36	114 43.96	10277.3	979194.66	109.36	5.61	25.44	-216.83	-15.89
03L046	38 39.99	114 44.89	9028.2	979284.11	82.03	5.74	14.44	-212.80	-11.50
03L047	38 34.64	114 50.82	6505.6	979450.26	19.03	0.51	1.58	-202.78	-3.52

03L048	38 31.41	114 50.66	6288.8	979464.18	17.32	0.77	2.49	-196.18	1.62
03L049	38 30.60	114 44.05	7995.7	979346.40	61.12	4.20	9.81	-203.24	-5.53
03L050	38 32.95	114 44.26	8564.2	979304.18	68.86	10.91	20.61	-204.03	-5.52
03L051	38 34.46	114 45.52	6916.2	979418.62	26.24	2.54	4.34	-206.82	-7.11
03L052	38 36.56	114 44.03	9196.9	979263.68	82.49	7.79	21.29	-211.22	-11.38
03L053	38 37.51	114 43.72	9316.6	979261.72	90.38	4.39	17.70	-210.98	-10.77
03L054	38 39.09	114 43.80	9804.6	979229.65	101.82	4.77	20.67	-213.12	-12.41
03L055	38 38.10	114 43.68	9812.3	979225.29	99.64	6.59	24.18	-212.06	-11.79
03L056	38 34.06	114 52.33	6831.7	979431.45	31.71	0.69	1.98	-200.82	-2.20
03L057	38 29.29	114 45.78	6871.4	979422.68	33.68	2.90	4.37	-197.82	-0.47
03L058	38 27.78	114 46.07	6632.6	979436.22	27.00	1.54	2.64	-198.09	-1.40
03L059	38 26.85	114 44.79	7345.9	979378.29	37.46	2.49	5.26	-209.32	-13.13
03L060	38 24.40	114 47.23	6449.6	979438.22	16.76	1.02	1.70	-203.01	-8.03
03L061	38 18.73	114 49.89	7019.8	979400.64	41.08	2.62	5.20	-194.65	-3.16
03L062	38 14.92	114 52.21	6361.5	979442.43	26.60	0.98	1.82	-190.06	-0.69
03L063	38 11.99	114 53.88	7006.7	979393.63	42.72	1.99	4.97	-192.79	-5.45
03L064	38 11.37	114 56.67	7057.0	979389.48	44.21	3.59	7.23	-190.77	-4.12
03L065	38 17.16	114 55.35	6263.7	979442.86	14.55	0.50	0.99	-199.59	-9.57
04L001	38 31.23	115 12.57	5337.0	979520.01	-16.04	0.03	0.50	-199.01	-4.69
04L002	38 31.10	115 11.49	5304.3	979523.56	-15.37	0.02	0.36	-197.36	-2.95
04L003	38 31.10	115 10.34	5270.8	979519.90	-22.18	0.01	0.27	-203.11	-8.50
04L004	38 31.11	115 09.47	5250.5	979515.95	-28.05	0.01	0.23	-208.33	-13.62
04L005	38 31.13	115 08.42	5265.6	979514.16	-28.45	0.02	0.21	-209.27	-14.43
04L006	38 31.16	115 07.28	5254.5	979510.32	-33.38	0.01	0.21	-213.82	-18.75
04L007	38 31.16	115 06.15	5252.4	979503.42	-40.48	0.02	0.26	-220.80	-25.58
04L008	38 31.16	115 04.46	5258.7	979493.98	-49.33	0.01	0.36	-229.75	-34.21
04L009	38 31.16	115 03.31	5290.8	979489.46	-50.83	0.02	0.49	-232.23	-36.55
04L010	38 31.16	115 02.22	5352.0	979485.76	-48.78	0.03	0.65	-232.11	-36.26
04L011	38 35.69	114 40.69	6330.1	979448.85	-0.42	0.17	1.75	-216.07	-15.14
04L012	38 35.87	114 41.78	6640.1	979432.64	12.24	0.43	2.76	-212.98	-12.21
04L013	38 35.55	114 43.66	7412.5	979389.62	42.27	1.90	4.66	-207.38	-7.15
04L014	38 35.35	114 44.81	6941.0	979417.75	26.39	2.63	4.79	-207.07	-6.87
04L015	38 35.25	114 45.27	6747.9	979430.20	20.84	1.68	3.80	-207.01	-6.84
04L016	38 35.62	114 46.21	6434.2	979444.86	5.48	0.37	2.30	-213.18	-12.77
04L017	38 35.32	114 46.65	6378.6	979449.02	4.85	0.13	1.67	-212.53	-12.29
04L018	38 50.04	114 49.71	7245.3	979407.20	22.82	0.08	1.22	-224.57	-18.92
04L019	38 50.46	114 50.63	7309.8	979403.54	24.60	0.06	1.28	-224.92	-19.27
04L020	38 50.55	114 52.53	7461.9	979403.27	38.49	0.19	2.01	-215.50	-10.05
04L021	38 50.02	114 53.07	7560.8	979395.25	40.55	0.47	2.49	-216.33	-11.22
04L022	38 49.33	114 53.03	7543.1	979396.23	40.88	0.60	2.46	-215.42	-10.60
04L023	38 47.85	114 53.44	7681.1	979387.76	47.55	0.40	2.34	-213.57	-9.39
04L024	38 47.77	114 52.38	7534.1	979392.71	38.81	0.31	1.85	-217.80	-13.41
04L025	38 47.81	114 51.37	7391.1	979395.14	27.75	0.22	1.49	-224.35	-19.82
04L026	38 44.98	114 50.10	6804.3	979426.50	8.13	0.29	1.68	-223.77	-19.88
04L027	38 44.53	114 52.13	6910.9	979425.22	17.53	0.75	1.97	-217.72	-14.35
04L028	38 35.39	114 48.91	6305.2	979459.53	8.36	0.09	1.08	-207.11	-7.10
04L029	38 35.50	114 50.18	6406.0	979456.93	15.07	0.18	1.10	-203.81	-3.97
04L030	38 35.86	114 52.27	6588.9	979443.53	18.33	0.07	1.00	-206.90	-7.29
04L031	38 35.36	114 52.98	6712.8	979436.52	23.70	0.20	1.20	-205.56	-6.38
04L032	38 34.95	114 53.53	6799.1	979428.44	24.33	0.41	1.49	-207.58	-8.75
04L033	38 34.37	114 54.15	6966.3	979415.23	27.69	0.18	1.43	-209.99	-11.64
04L034	38 33.92	114 54.67	6805.9	979421.95	20.00	0.68	2.00	-211.64	-13.53
04L035	38 32.46	114 56.03	6437.3	979451.65	17.20	1.11	3.52	-200.34	-3.03
04L036	38 32.19	114 57.01	6228.1	979466.71	13.00	1.00	3.37	-197.55	-0.48
04L037	38 32.19	114 58.01	6055.9	979476.67	6.78	0.91	2.75	-198.51	-1.60
04L038	38 32.02	114 59.00	5808.3	979487.84	-5.07	0.14	1.73	-202.92	-6.17
04L039	38 31.69	115 00.06	5595.3	979494.52	-17.93	0.07	1.25	-208.98	-12.55
04L040	38 31.36	115 01.11	5434.9	979490.97	-36.07	0.04	0.91	-221.97	-25.83

04L041	38 31.19	115 01.65	5378.9	979487.13	-44.92	0.03	0.77	-229.05	-33.04
04L042	38 31.49	115 00.70	5495.5	979493.22	-28.31	0.06	1.04	-216.16	-19.90
04L043	38 31.83	114 59.60	5691.3	979492.17	-11.46	0.09	1.42	-205.62	-9.06
04L044	38 37.16	114 50.88	6530.4	979449.28	16.67	0.04	0.90	-206.66	-6.21
04L045	38 46.99	114 50.56	6999.0	979414.63	11.60	0.40	1.60	-227.02	-22.51
04L046	38 46.47	114 51.93	7501.4	979386.94	31.88	0.91	2.36	-223.10	-19.17
04L047	38 46.38	114 48.72	7101.7	979412.32	19.84	0.72	2.03	-221.85	-17.42
04L048	38 46.56	114 47.53	7322.4	979402.61	30.60	1.16	2.55	-218.09	-13.60
04L049	38 43.15	114 50.70	6682.3	979437.29	10.15	0.14	1.46	-217.81	-14.75
04L050	38 42.59	114 49.87	6828.6	979425.85	13.28	0.19	1.49	-219.64	-16.75
04L051	38 40.09	114 50.05	6489.7	979448.37	7.63	0.08	1.35	-213.87	-11.96
04L052	38 37.72	114 48.64	6354.6	979454.94	4.99	0.02	1.33	-211.92	-10.84
04L053	38 38.77	114 48.10	6542.0	979446.17	12.29	0.19	1.84	-210.50	-8.97
04L054	38 38.23	114 47.96	6436.9	979451.77	8.81	0.14	1.81	-210.43	-9.05
04L055	38 37.23	114 47.52	6379.5	979451.26	4.37	0.09	1.75	-212.97	-12.00
04L056	38 35.95	114 47.13	6309.5	979453.38	1.79	0.07	1.62	-213.28	-12.78
04L057	38 34.30	114 47.31	6211.1	979459.51	1.10	0.04	1.27	-210.97	-11.27
04L058	38 32.59	114 47.11	6139.2	979460.46	-2.19	0.04	1.22	-211.86	-12.85
04L059	38 30.98	114 47.15	6105.4	979460.65	-2.81	0.05	1.09	-211.45	-13.22
04L060	38 28.13	114 47.89	6057.4	979460.03	-3.76	0.03	0.75	-211.10	-14.32
04L061	38 26.33	114 48.47	6013.5	979468.31	3.04	0.06	0.70	-202.85	-6.98
04L062	38 26.32	114 47.62	6078.0	979473.34	14.14	0.74	1.44	-193.21	2.79
04L063	38 26.67	114 49.47	6003.7	979454.50	-12.19	0.01	0.51	-217.93	-22.04
04L064	38 24.85	114 48.64	6011.1	979474.12	10.79	0.45	0.97	-194.74	0.38
04L065	38 22.32	114 49.25	6005.8	979474.74	14.63	1.44	1.98	-189.72	4.06
04L066	38 20.33	114 50.87	6041.1	979466.19	12.31	0.59	1.51	-193.71	-1.19
04L067	38 32.92	114 48.94	6149.3	979468.07	5.88	0.15	1.45	-203.90	-5.00
04L068	38 31.75	114 49.50	6091.4	979472.32	6.41	0.11	1.50	-201.34	-3.07
04L069	38 27.80	114 52.95	6024.0	979473.90	7.46	0.06	1.23	-198.27	-2.52
04L070	38 24.97	114 53.91	5982.1	979467.60	1.37	0.01	0.65	-203.50	-9.31
04L071	38 24.35	114 55.46	6238.1	979460.84	19.58	1.08	1.89	-192.79	0.74
04L072	38 24.31	114 55.33	6180.0	979464.28	17.62	0.80	1.61	-193.05	0.52
04L073	38 24.26	114 55.20	6121.1	979467.48	15.36	0.59	1.41	-193.50	0.07
04L074	38 24.21	114 55.06	6098.7	979468.53	14.38	0.38	1.19	-193.94	-0.36
04L075	38 24.17	114 54.92	6075.4	979471.35	15.06	0.27	1.06	-192.58	1.01
04L076	38 24.12	114 54.78	6050.6	979470.17	11.63	0.19	0.96	-195.27	-1.64
04L077	38 24.07	114 54.63	6028.3	979470.79	10.22	0.16	0.91	-195.97	-2.35
04L078	38 24.03	114 54.53	6000.0	979471.89	8.72	0.10	0.83	-196.57	-2.94
04L079	38 23.99	114 54.40	5984.0	979471.84	7.23	0.06	0.76	-197.59	-3.96
04L080	38 23.89	114 54.12	5977.4	979469.39	4.31	0.02	0.63	-200.42	-6.76
04L081	38 23.75	114 53.71	5978.7	979464.81	0.05	0.02	0.53	-204.82	-11.14
04L082	38 23.58	114 53.21	5977.4	979459.71	-4.92	0.01	0.44	-209.83	-16.15
04L083	38 23.35	114 52.57	5974.7	979454.76	-9.79	0.01	0.39	-214.66	-20.96
04L084	38 23.13	114 51.95	5973.3	979451.65	-12.71	0.01	0.37	-217.55	-23.86
04L085	38 22.97	114 51.49	5972.0	979450.92	-13.32	0.01	0.37	-218.12	-24.42
04L086	38 22.79	114 50.96	5974.3	979451.69	-12.07	0.01	0.40	-216.92	-23.20
04L087	38 22.65	114 50.55	5977.9	979454.22	-9.00	0.01	0.45	-213.92	-20.22
04L088	38 22.53	114 50.23	5979.2	979459.23	-3.69	0.03	0.53	-208.57	-14.86
04L089	38 22.48	114 50.08	5980.9	979462.03	-0.66	0.06	0.59	-205.54	-11.83
04L090	38 22.27	114 50.32	5979.0	979460.65	-1.91	0.03	0.56	-206.76	-13.21
04L091	38 22.40	114 49.86	5979.4	979466.46	3.75	0.16	0.71	-200.96	-7.27
04L092	38 22.33	114 49.66	5975.6	979470.77	7.81	0.34	0.91	-196.57	-2.85
04L093	38 22.26	114 49.44	5981.9	979473.66	11.39	0.67	1.24	-192.88	0.86
04L094	38 22.20	114 49.29	6003.0	979473.76	13.56	0.99	1.56	-191.11	2.60
04L095	38 22.14	114 49.11	6045.6	979471.70	15.59	1.32	1.88	-190.22	3.49
04L096	38 22.09	114 48.94	6100.5	979468.71	17.84	1.35	1.90	-189.83	3.85
04L097	37 26.25	114 44.18	5892.3	979419.52	30.66	0.26	1.78	-170.01	-9.36
04L098	37 25.48	114 44.29	5772.6	979426.45	27.46	0.52	1.99	-168.90	-8.96

04L099	37 25.97	114 45.04	5667.7	979428.72	19.16	0.93	2.38	-173.24	-12.87
04L100	37 26.30	114 45.75	5557.5	979434.42	14.02	1.34	2.77	-174.21	-13.58
04L101	37 26.52	114 46.22	5485.9	979437.92	10.47	1.71	3.15	-174.94	-14.14
04L102	37 26.52	114 46.99	5379.1	979444.86	7.37	1.76	3.08	-174.45	-13.69
04L103	37 26.93	114 50.40	4889.4	979461.31	-22.80	0.05	0.74	-190.21	-29.28
04L104	37 19.68	114 53.02	4665.6	979474.54	-20.07	0.02	0.65	-179.91	-25.78
04L105	37 19.82	114 54.12	4603.3	979477.79	-22.88	0.02	0.55	-180.68	-26.44
04L106	37 19.02	114 55.77	4532.3	979481.93	-24.25	0.01	0.51	-179.66	-26.22
04L107	37 19.60	114 57.11	4542.8	979484.48	-21.55	0.02	0.43	-177.40	-23.44
04L108	37 18.75	114 56.23	4543.5	979482.29	-22.44	0.01	0.50	-178.25	-25.06
04L109	37 19.55	114 56.07	4536.7	979480.02	-26.51	0.00	0.43	-182.15	-28.22
04L110	37 39.69	114 44.40	5016.9	979491.57	0.86	0.23	0.83	-170.83	-0.07
04L111	37 41.28	114 44.94	4774.4	979499.16	-16.66	0.08	0.58	-180.30	-8.54
04L112	37 42.09	114 44.55	4788.3	979501.51	-14.19	0.11	0.61	-178.27	-6.01
04L113	37 42.91	114 44.15	4772.1	979506.56	-11.86	0.34	0.85	-175.14	-2.35
04L114	37 44.16	114 43.52	4853.0	979507.11	-5.52	0.17	0.70	-171.74	1.85
04L115	37 45.05	114 43.04	4829.6	979510.21	-5.92	0.63	1.16	-170.87	3.38
04L116	37 45.81	114 42.63	4955.6	979503.73	-1.67	0.93	1.41	-170.68	4.07
04L117	37 47.25	114 41.18	4991.3	979502.23	-1.91	0.21	0.70	-172.85	3.08
04L118	37 47.36	114 40.27	5085.9	979494.96	-0.45	0.08	0.63	-174.70	1.42
04L119	37 47.20	114 39.38	5188.4	979487.27	1.73	0.11	0.70	-175.95	0.28
04L120	37 46.58	114 37.22	5375.6	979478.36	11.32	0.12	0.75	-172.72	3.48
04L121	37 47.58	114 36.20	5571.4	979466.60	16.50	0.28	1.00	-173.98	3.08
04L122	37 48.06	114 35.04	5736.4	979454.69	19.40	0.08	0.91	-176.82	0.70
04L123	37 48.64	114 34.58	5882.3	979454.69	32.26	0.12	1.17	-168.67	9.28
04L124	37 49.34	114 34.94	6060.2	979436.36	29.63	0.35	1.73	-176.82	1.38
04L125	37 49.31	114 34.21	6093.9	979436.65	33.13	0.68	2.10	-174.10	4.24
04L126	37 51.22	114 36.00	6373.2	979420.44	40.38	1.98	4.34	-174.15	4.95
04L127	37 51.60	114 36.09	6442.4	979416.91	42.80	1.69	4.29	-174.15	5.10
04L128	37 52.56	114 35.80	6887.2	979387.82	54.11	3.68	7.30	-175.01	4.77
04L129	37 52.93	114 36.37	6649.6	979404.16	47.58	2.17	5.57	-175.16	4.81
04L130	37 54.10	114 36.46	6743.7	979397.80	48.35	2.51	5.97	-177.20	3.43
04L131	37 54.56	114 36.33	6846.3	979392.15	51.67	2.63	6.17	-177.17	3.71
04L132	37 54.99	114 35.94	7037.0	979378.41	55.22	5.00	8.61	-177.68	3.49
04L133	37 55.59	114 36.34	6891.6	979389.78	52.05	1.69	4.84	-179.67	1.86
04L134	37 54.99	114 36.78	6603.6	979407.81	43.89	0.86	3.88	-178.96	2.18
04L135	37 55.10	114 37.46	6323.9	979426.10	35.74	0.34	2.73	-178.72	2.40
04L136	37 55.13	114 38.29	6065.5	979439.15	24.46	0.25	2.10	-181.81	-0.75
04L137	37 54.50	114 39.24	5751.0	979456.60	13.27	0.19	1.68	-182.67	-2.13
04L138	37 53.21	114 39.89	5423.6	979480.87	8.66	0.37	1.57	-176.20	3.54
04L139	37 52.16	114 39.60	5370.5	979482.96	7.29	0.13	1.30	-176.02	3.14
04L140	37 51.82	114 38.95	5498.7	979474.51	11.39	0.15	1.46	-176.15	2.92
04L141	37 51.16	114 39.67	5303.6	979485.12	4.62	0.12	1.15	-176.56	1.98
04L142	37 50.65	114 41.42	4951.5	979499.26	-13.59	0.06	0.70	-183.16	-5.15
04L143	37 52.10	114 43.24	4747.4	979509.54	-24.61	0.07	0.59	-187.31	-8.78
04L144	37 58.83	114 41.13	5170.3	979492.44	-11.80	0.21	1.18	-188.38	-5.44
04L145	37 58.48	114 38.21	5913.8	979446.75	12.91	0.30	2.04	-188.24	-5.08
04L146	37 58.36	114 37.09	6323.5	979424.69	29.53	0.75	2.94	-184.71	-1.51
04L147	37 58.62	114 36.10	6766.3	979397.24	43.31	2.16	4.64	-184.34	-0.85
04L148	38 04.91	114 44.81	5114.5	979494.81	-23.56	0.02	0.43	-198.99	-13.30
04L149	38 11.21	114 47.23	5482.3	979483.06	-9.97	0.05	0.37	-198.03	-9.48
04L150	38 11.78	114 48.04	5422.8	979485.39	-14.06	0.04	0.38	-200.09	-11.34
04L151	38 13.35	114 50.86	5696.7	979470.59	-5.42	0.18	0.82	-200.36	-11.39
04L152	38 13.95	114 52.53	6159.9	979454.26	20.90	0.75	1.49	-189.20	-0.31
04L153	38 13.99	114 53.57	6324.6	979443.96	26.02	0.44	1.22	-189.97	-1.27
04L154	38 14.67	114 55.23	6084.5	979455.60	14.10	0.06	0.55	-194.36	-5.53
04L155	38 15.42	114 56.73	5916.8	979465.10	6.74	0.03	0.40	-196.14	-7.08
04L156	38 15.93	114 57.87	5925.8	979464.02	5.76	0.07	0.40	-197.44	-8.31

04L157	38 07.50	114 49.63	5110.6	979502.49	-20.04	0.08	0.41	-195.35	-9.18
04L158	38 06.29	114 49.62	5095.3	979499.39	-22.81	0.03	0.28	-197.72	-12.23
04L159	38 05.69	114 49.33	5068.2	979499.31	-24.56	0.03	0.27	-198.55	-13.34
04L160	38 05.06	114 48.92	5042.5	979501.72	-23.64	0.03	0.27	-196.76	-11.80
04L161	38 04.41	114 48.60	5016.3	979506.53	-20.34	0.03	0.26	-192.57	-7.92
04L162	38 03.96	114 48.82	4999.8	979509.78	-17.98	0.01	0.24	-189.67	-5.29
04L163	38 02.29	114 50.72	5105.9	979506.22	-9.13	0.04	0.30	-184.39	-1.29
04L164	38 02.88	114 47.44	4946.7	979502.67	-28.51	0.03	0.28	-198.34	-14.30
04L165	38 01.55	114 46.39	4890.1	979502.00	-32.55	0.02	0.31	-200.42	-16.95
04L166	38 00.80	114 45.97	4851.9	979504.74	-32.30	0.01	0.33	-198.84	-15.69
04L167	37 59.80	114 49.06	4854.0	979518.34	-17.04	0.03	0.37	-183.62	-1.63
04L168	37 58.94	114 49.29	4853.3	979517.82	-16.37	0.03	0.37	-182.92	-1.46
04L169	37 47.27	114 50.59	4667.7	979511.04	-23.55	0.03	0.40	-183.72	-9.21
04L170	37 42.47	114 51.22	4813.9	979495.20	-18.65	0.04	0.42	-183.79	-12.25
04L171	37 41.72	114 52.94	5077.1	979482.97	-5.04	0.09	0.63	-178.99	-8.18
04L172	37 40.99	114 52.99	5051.4	979485.00	-4.36	0.16	0.69	-177.37	-6.98
04L173	37 41.81	114 54.42	5307.5	979476.43	9.94	0.26	1.13	-171.38	-0.70
04L174	37 41.90	114 55.19	5422.0	979471.07	15.21	0.49	1.59	-169.57	1.02
04L175	37 42.31	114 55.71	5547.5	979461.32	16.66	1.29	2.32	-171.68	-0.92
04L176	37 42.63	114 56.27	5680.1	979450.02	17.36	2.29	3.25	-174.59	-3.73
04L177	37 43.79	114 56.90	5851.1	979439.51	21.23	0.50	1.47	-178.35	-6.89
04L178	37 44.45	114 57.20	5793.2	979443.71	19.02	0.56	1.44	-178.60	-6.71
04L179	37 45.05	114 58.01	5571.1	979458.41	11.97	0.27	0.99	-178.51	-6.29
04L180	37 45.50	114 58.65	5453.6	979465.70	7.56	0.31	0.93	-178.96	-6.45
04L181	37 45.06	114 59.90	5335.5	979470.44	1.84	0.09	0.61	-180.96	-8.70
04L182	37 43.76	114 59.82	5270.0	979477.98	5.12	0.61	1.23	-174.82	-3.35
04L183	37 36.73	114 43.41	5673.5	979443.44	18.76	0.36	1.35	-174.87	-6.02
04L184	37 36.35	114 44.23	5663.9	979444.49	19.46	0.50	1.52	-173.66	-5.21
04L185	37 35.93	114 44.57	5780.1	979434.97	21.47	0.53	1.65	-175.50	-7.35
04L186	37 34.50	114 45.28	5829.9	979425.16	18.43	0.38	1.66	-180.23	-13.19
04L187	37 33.65	114 46.30	5934.9	979415.36	19.73	0.49	1.93	-182.24	-15.98
04L188	37 34.26	114 46.34	5774.7	979427.40	15.83	0.44	1.66	-180.94	-14.25
04L189	37 33.22	114 47.25	5735.6	979425.06	11.33	0.19	1.45	-184.32	-18.42
04L190	37 32.73	114 48.48	5495.4	979432.81	-2.78	0.14	1.12	-190.55	-25.05
04C001	37 37.66	114 30.57	4443.3	979515.13	-26.54	1.14	2.33	-177.08	-5.02
04C002	37 40.11	114 29.29	4603.4	979502.29	-27.90	0.22	1.17	-185.09	-11.14
04C003	37 39.58	114 29.61	4479.1	979509.40	-31.70	0.54	1.81	-183.99	-10.40
04C004	37 36.50	114 50.97	4838.2	979473.28	-29.58	0.02	0.37	-195.61	-27.70
04C005	37 35.93	114 51.32	4850.9	979471.41	-29.42	0.01	0.36	-195.89	-28.36
04C006	37 35.55	114 51.52	4857.9	979470.36	-29.26	0.02	0.38	-195.96	-28.70
04C007	37 36.29	114 50.75	4867.6	979471.30	-28.49	0.03	0.39	-195.51	-27.70
04C008	37 35.27	114 51.04	4917.5	979467.65	-25.96	0.03	0.41	-194.66	-27.53
04C009	37 36.50	114 50.06	4906.0	979470.13	-26.36	0.03	0.40	-194.68	-26.68
04C010	37 36.51	114 49.27	4981.0	979465.68	-23.77	0.04	0.46	-194.60	-26.50
04C011	37 36.51	114 48.50	5050.0	979463.85	-19.11	0.06	0.56	-192.20	-24.02
04C012	37 33.10	114 48.29	5525.5	979433.69	0.39	0.12	1.09	-188.43	-22.65
04C013	37 14.79	114 58.16	4257.9	979507.52	-18.31	2.43	3.76	-161.07	-11.59
04C014	37 15.25	114 57.76	4403.3	979497.28	-15.55	1.01	2.21	-164.84	-14.96
04C015	37 15.63	114 57.42	4675.7	979478.49	-9.28	0.29	1.31	-168.81	-18.66
04C016	37 16.14	114 57.17	4620.6	979480.71	-12.98	0.12	1.02	-170.91	-20.27
04C017	37 17.24	114 56.64	4573.6	979483.44	-16.27	0.04	0.73	-172.88	-21.16
04C018	37 17.76	114 56.99	4549.3	979486.14	-16.61	0.03	0.60	-172.51	-20.26
04C019	37 18.38	114 57.27	4539.9	979484.24	-20.29	0.01	0.50	-175.98	-23.17
04C020	37 18.74	114 57.11	4541.5	979483.80	-21.11	0.01	0.47	-176.88	-23.73
04C021	37 18.60	114 57.66	4535.9	979485.44	-19.79	0.04	0.50	-175.33	-22.31
04C022	37 18.93	114 57.88	4539.1	979486.55	-18.86	0.11	0.55	-174.46	-21.14
04C023	37 20.34	114 58.13	4577.6	979483.03	-20.81	0.15	0.56	-177.72	-23.10
04C024	37 21.12	114 58.26	4656.3	979479.28	-18.29	0.18	0.64	-177.83	-22.55

04C025	37 35.82	114 43.63	6294.4	979397.82	32.82	2.58	4.53	-178.83	-10.87
04C026	37 35.89	114 41.99	6337.8	979395.15	34.13	1.07	2.84	-180.70	-12.40
04C027	37 35.33	114 44.60	6098.3	979411.93	29.21	0.80	2.36	-177.91	-10.28
04C028	37 36.02	114 44.80	5994.2	979423.91	30.40	1.00	2.51	-173.02	-4.93
04C029	37 34.75	114 42.87	6758.6	979362.93	43.11	1.40	4.55	-184.36	-17.14
04C030	37 32.85	114 45.64	6730.2	979361.12	41.40	3.32	6.80	-182.85	-17.33
04C031	37 31.52	114 44.82	6804.8	979355.94	45.17	1.27	4.49	-183.94	-19.31
04C032	37 31.52	114 46.24	6941.1	979344.14	46.18	5.15	10.09	-181.98	-17.60
04C033	37 30.06	114 45.70	6924.0	979341.91	44.46	7.87	12.35	-180.85	-17.53
04C034	37 27.36	114 44.49	6409.8	979382.71	40.87	2.20	4.52	-174.72	-13.31
04C035	37 26.38	114 44.47	6135.1	979402.71	36.48	1.08	2.83	-171.43	-10.80
04C036	37 24.64	114 46.70	6524.5	979368.34	41.24	6.56	10.84	-171.96	-13.25
04C037	37 23.40	114 46.60	5907.6	979412.33	29.06	1.75	3.76	-170.16	-12.38
04C038	37 22.57	114 47.00	5722.9	979419.99	20.56	2.42	4.21	-171.89	-14.91
04C039	37 21.48	114 47.18	5758.7	979409.90	15.42	2.06	3.95	-178.51	-22.61
04C040	37 19.72	114 47.88	6692.7	979345.96	41.82	7.45	13.71	-174.25	-20.47
04C041	37 18.06	114 48.01	5552.2	979421.12	12.20	0.95	2.82	-175.81	-23.39
04C042	37 19.34	114 50.32	5239.3	979440.90	0.71	1.84	3.06	-176.35	-22.64
04C043	37 18.30	114 51.13	5659.8	979414.14	14.99	3.58	5.91	-173.61	-21.08
04C044	37 17.48	114 51.64	5842.8	979404.53	23.77	4.80	7.73	-169.26	-17.62
04C045	37 17.81	114 52.95	5483.9	979430.41	15.44	3.64	5.55	-167.51	-15.46
04C046	37 20.65	114 55.84	4710.5	979466.28	-25.52	1.37	1.88	-185.66	-30.72
04C047	37 17.15	114 55.88	4637.6	979482.09	-11.47	0.07	0.97	-170.04	-18.40
04C048	37 16.15	114 56.38	4639.6	979480.95	-10.97	0.18	1.24	-169.33	-18.71
04C049	37 14.52	114 56.90	5804.8	979401.07	21.04	3.61	8.40	-170.02	-21.25
04C050	37 14.52	114 58.74	4986.9	979455.74	-1.17	4.52	6.46	-166.20	-17.12
04C051	37 15.45	115 00.10	5795.9	979397.56	15.34	5.56	12.06	-171.76	-21.96
04C052	37 16.25	114 59.30	5507.3	979418.68	8.17	3.88	7.48	-173.63	-23.08
04C053	37 16.91	114 58.43	5224.7	979440.72	2.69	1.65	3.65	-173.29	-22.02
04C054	37 17.65	114 59.36	5060.0	979452.50	-2.08	1.27	2.84	-173.23	-21.21
04C055	37 22.79	114 56.74	4730.8	979475.05	-17.95	0.37	0.86	-179.81	-23.01
04C056	37 21.66	114 56.96	4643.0	979478.68	-20.93	0.40	0.83	-179.82	-24.01
04C057	37 19.79	114 59.21	5012.0	979452.44	-9.77	2.41	3.64	-178.47	-24.51
04C058	37 21.20	114 59.69	4994.1	979456.00	-9.94	1.72	2.81	-178.86	-23.62
04C059	37 25.26	115 00.51	6368.2	979373.00	30.31	7.61	13.01	-175.39	-17.14
04C060	37 26.61	115 00.15	6073.4	979399.36	27.00	2.45	5.42	-176.22	-16.71
04C061	37 27.92	114 59.11	5801.2	979411.85	12.00	0.50	2.48	-184.86	-24.23
04C062	37 28.00	114 56.80	5707.6	979413.22	4.46	3.86	6.10	-185.58	-24.67
04C063	37 29.09	114 58.40	5925.3	979400.62	10.73	2.96	5.33	-187.51	-25.93
04C064	37 28.70	115 00.46	6001.4	979404.77	22.60	1.04	3.59	-179.99	-18.84
04C065	37 30.92	115 00.76	5685.5	979426.99	11.90	1.44	3.46	-180.02	-17.17
04C066	37 32.97	114 54.40	5110.4	979451.99	-20.14	1.14	1.50	-194.36	-29.29
04C067	37 33.26	114 59.84	5462.2	979435.10	-4.39	1.75	2.75	-189.39	-24.70
04C068	37 34.96	115 00.72	5391.4	979448.38	-0.24	0.99	1.80	-183.76	-17.91
04C069	37 36.51	115 00.71	5223.6	979461.63	-5.02	0.52	1.02	-183.58	-16.66
04C070	37 37.41	114 54.00	5213.6	979457.39	-11.51	0.58	0.96	-189.80	-21.76
04C071	37 40.33	114 52.41	5535.5	979445.35	2.45	2.17	3.14	-184.66	-14.82
04C072	37 40.68	114 56.70	6535.8	979387.70	38.30	0.88	4.44	-181.68	-12.29
04C073	37 42.66	114 54.61	5993.0	979428.49	25.19	2.62	4.31	-176.39	-5.48
04C074	37 44.59	114 56.33	6002.5	979431.83	26.61	0.54	1.77	-177.84	-5.90
04C075	37 45.75	114 56.59	6561.0	979391.16	36.73	3.67	6.94	-181.61	-9.20
04C076	37 46.87	114 56.91	6622.6	979386.43	36.16	4.78	8.41	-182.82	-9.80
04C077	37 45.25	114 54.51	5990.6	979429.43	22.13	4.57	6.19	-177.49	-5.03
04C078	38 00.13	114 49.38	5004.0	979511.55	-10.22	0.47	0.72	-181.57	0.51
04C079	37 59.86	114 52.46	5924.3	979446.29	11.42	1.76	2.85	-189.28	-8.12
04C080	37 58.72	114 53.38	6434.0	979411.34	26.03	2.73	5.60	-189.31	-9.05
04C081	37 57.61	114 53.55	6292.6	979419.99	23.02	2.68	5.07	-188.03	-8.39
04C082	37 57.21	114 54.36	6169.7	979429.69	21.75	2.30	4.14	-186.03	-6.63

04C083	37 56.46	114 51.96	5550.4	979470.24	5.19	1.59	2.23	-183.33	-3.90
04C084	37 53.30	114 55.72	6551.8	979398.39	32.08	4.40	8.00	-184.89	-8.03
04C085	37 52.52	114 56.00	6419.6	979408.23	30.63	3.52	6.38	-183.44	-6.99
04C086	37 49.12	114 56.53	6121.0	979427.75	27.05	2.12	3.76	-179.45	-4.93
04C087	37 47.89	114 56.38	6562.0	979393.99	36.53	4.42	7.82	-180.96	-7.27
04C088	37 43.62	114 54.11	5579.6	979456.82	13.27	0.93	1.80	-176.70	-5.04
04C089	37 58.31	114 40.64	5689.1	979462.65	7.94	1.83	3.02	-184.55	-2.02
04C090	37 56.47	114 40.13	6618.1	979402.26	37.54	5.93	9.97	-179.72	1.50
04C092	37 55.72	114 41.36	5762.7	979456.97	12.96	3.45	5.02	-180.04	0.78
04C093	37 54.88	114 41.36	5729.8	979457.96	12.09	4.00	5.50	-179.31	1.00
04C094	37 54.13	114 41.05	5408.7	979480.82	5.86	1.11	2.17	-177.89	2.16
04C095	37 50.21	114 38.02	6105.3	979436.50	32.74	1.99	3.76	-173.23	4.83
04C096	37 49.14	114 36.91	6182.4	979431.06	36.11	1.76	3.38	-172.88	4.71
04C097	37 46.50	114 33.56	6139.1	979433.87	38.70	1.73	3.21	-168.97	7.77
04C098	37 36.74	114 47.17	5060.1	979475.16	-7.19	0.24	0.94	-180.24	-11.76
04C099	37 34.29	114 48.37	5355.1	979442.36	-8.69	0.10	0.86	-191.92	-25.31
04C100	37 28.93	114 50.23	4988.1	979454.18	-23.56	0.06	0.75	-194.34	-31.78
04C101	37 28.32	114 50.34	4961.4	979456.66	-22.71	0.06	0.75	-192.58	-30.56
04C102	37 20.10	114 50.92	4802.5	979467.65	-14.70	0.06	0.94	-178.94	-24.32
04C103	37 20.59	114 50.44	4870.2	979463.10	-13.60	0.12	1.05	-180.04	-24.94
04C104	37 17.78	114 49.72	4996.4	979454.73	-6.02	0.06	1.31	-176.53	-24.30
04C105	37 17.17	114 47.28	5545.7	979421.92	13.69	1.33	3.42	-173.50	-22.05
04C106	37 17.17	114 47.88	5367.7	979433.90	8.94	0.71	2.61	-172.97	-21.44
04C107	37 17.48	114 48.45	5213.1	979442.47	2.52	0.44	2.08	-174.62	-22.75
04C108	37 14.64	114 50.26	5431.5	979439.00	23.71	1.28	2.83	-160.16	-11.36
04C109	37 13.86	114 52.48	5105.0	979460.22	15.37	0.31	1.53	-158.63	-10.50
04C110	37 14.11	114 51.96	5102.8	979462.88	17.46	0.30	1.55	-156.44	-8.09
04C111	37 14.35	114 51.51	5165.2	979460.99	21.09	0.46	1.73	-154.77	-6.21
04C112	37 14.68	114 51.17	5222.9	979455.24	20.28	0.54	1.82	-157.46	-8.55
04C113	37 14.93	114 50.86	5283.6	979449.52	19.90	0.59	1.92	-159.81	-10.64
04C114	37 15.31	114 50.66	5364.1	979444.38	21.78	0.57	1.99	-160.63	-11.13
04C115	37 15.78	114 50.36	5298.4	979444.96	15.50	0.52	1.87	-164.77	-14.75
04C116	37 16.24	114 50.12	5165.1	979452.42	9.76	0.53	1.85	-165.97	-15.43
04C117	37 17.24	114 50.26	5004.1	979455.78	-3.46	0.09	1.28	-174.26	-22.63
04C118	37 17.80	114 50.21	4957.3	979459.14	-5.32	0.15	1.26	-174.53	-22.28
04C119	37 18.85	114 50.18	4886.5	979465.24	-7.40	0.41	1.49	-173.95	-20.60
04C120	37 19.36	114 50.68	4833.5	979468.82	-9.54	0.35	1.31	-174.46	-20.61
04C121	37 19.39	114 51.53	4773.0	979470.27	-13.82	0.08	0.91	-177.07	-23.20
04C122	37 19.75	114 53.52	4634.4	979476.29	-21.35	0.01	0.59	-180.18	-25.99
04C123	37 19.89	114 54.63	4575.4	979478.29	-25.10	0.01	0.50	-182.00	-27.71
04C124	37 20.04	114 55.84	4538.9	979478.94	-28.10	0.01	0.43	-183.82	-29.40
04C125	37 20.41	114 56.32	4538.4	979484.36	-23.26	0.20	0.60	-178.79	-24.06
04C126	37 20.84	114 57.46	4598.2	979482.77	-19.86	0.06	0.48	-177.56	-22.47
04C127	37 22.10	114 58.10	4830.2	979469.19	-13.46	0.47	1.06	-178.53	-22.42
04C128	37 22.78	114 58.12	4879.5	979465.45	-13.56	0.28	0.93	-180.44	-23.73
04C129	37 23.28	114 58.06	4825.1	979468.47	-16.38	0.25	0.85	-181.47	-24.31
04C130	37 23.69	114 57.50	4770.6	979472.18	-18.39	0.09	0.65	-181.82	-24.25
04C131	37 23.95	114 56.90	4719.2	979478.23	-17.55	0.04	0.56	-179.31	-21.44
04C132	37 24.16	114 56.40	4667.4	979480.44	-20.51	0.12	0.60	-180.46	-22.39
04C133	37 20.79	114 56.21	4555.7	979483.02	-23.53	0.36	0.77	-179.49	-24.40
04C134	37 21.39	114 56.20	4543.8	979483.60	-24.94	0.46	0.87	-180.38	-24.72
04C135	37 22.02	114 56.12	4544.4	979482.86	-26.54	0.24	0.66	-182.22	-26.02
04C136	37 22.70	114 55.91	4552.8	979480.31	-29.29	0.32	0.75	-185.16	-28.30
04C137	37 23.26	114 55.82	4564.8	979479.58	-29.71	0.19	0.62	-186.12	-28.76
04C138	37 23.80	114 55.75	4604.6	979477.60	-28.73	0.13	0.56	-186.57	-28.76
04C139	37 24.05	114 54.02	4579.1	979467.81	-41.28	0.00	0.43	-198.37	-40.19
04C140	37 24.18	114 55.37	4607.0	979474.90	-31.76	0.02	0.45	-189.79	-31.62
04C141	37 24.62	114 56.19	4658.7	979479.12	-23.32	0.03	0.51	-183.06	-24.57

04C142	37 24.37	114 57.18	4768.5	979474.32	-17.43	0.05	0.62	-180.82	-22.63
04C143	37 24.67	114 56.76	4717.5	979478.51	-18.47	0.05	0.58	-180.16	-21.70
04C144	37 25.57	114 55.63	4649.8	979476.48	-28.18	0.03	0.51	-187.61	-28.27
04C145	37 26.06	114 54.27	4619.5	979470.45	-37.77	0.00	0.44	-196.24	-36.34
04C146	37 26.33	114 53.56	4636.3	979467.31	-39.72	0.00	0.45	-198.76	-38.59
04C147	37 26.11	114 52.35	4664.0	979463.92	-40.19	0.03	0.54	-200.08	-39.99
04C148	37 34.28	114 48.37	5360.1	979442.34	-8.23	0.09	0.85	-191.63	-25.03
04C149	37 26.11	114 52.36	4661.8	979463.94	-40.37	0.03	0.54	-200.19	-40.10
04C150	37 23.49	114 50.19	4777.5	979463.04	-26.59	0.05	0.85	-190.06	-32.13
04C151	37 24.23	114 50.03	4777.4	979464.10	-26.61	0.03	0.83	-190.09	-31.47
04C152	37 24.28	114 50.77	4721.5	979462.97	-33.07	0.02	0.71	-194.76	-36.14
04C153	37 24.74	114 52.08	4637.2	979462.99	-41.64	0.01	0.55	-200.61	-41.68
04C154	37 24.05	114 54.02	4572.0	979467.90	-41.86	0.01	0.44	-198.70	-40.51
04C155	37 19.88	114 54.63	4580.9	979478.40	-24.46	0.01	0.50	-181.55	-27.27
04C156	37 20.16	114 52.06	4710.5	979468.86	-22.22	0.01	0.70	-183.55	-28.89
04C157	37 19.25	114 52.28	4705.2	979473.62	-16.64	0.04	0.82	-177.66	-23.95
04C158	37 24.16	114 56.40	4668.4	979480.42	-20.44	0.11	0.59	-180.43	-22.36
04C159	37 22.10	114 58.09	4828.8	979469.12	-13.66	0.49	1.08	-178.66	-22.55
04C160	37 23.28	114 58.06	4825.7	979468.48	-16.31	0.25	0.85	-181.43	-24.27
04C161	37 23.69	114 57.50	4766.8	979472.17	-18.75	0.09	0.65	-182.06	-24.49
04C162	37 23.95	114 56.90	4714.9	979478.22	-17.96	0.04	0.56	-179.58	-21.71
04C163	37 25.53	114 56.42	4731.3	979477.32	-19.62	0.19	0.74	-181.61	-22.39
04C164	37 26.36	114 56.05	4722.7	979476.32	-22.63	0.08	0.64	-184.43	-24.48
04C165	37 26.91	114 55.70	4665.0	979478.78	-26.40	0.10	0.67	-186.19	-25.75
04C166	37 27.72	114 54.94	4691.7	979474.66	-29.18	0.02	0.54	-190.03	-28.87
04C167	37 28.11	114 54.54	4725.5	979471.68	-29.55	0.01	0.49	-191.61	-30.13
04C168	37 29.10	114 53.66	4766.4	979467.97	-30.86	0.01	0.44	-194.36	-31.97
04C169	37 30.00	114 52.95	4763.2	979469.72	-30.72	0.01	0.45	-194.11	-30.97
04C170	37 30.23	114 55.82	4961.3	979463.30	-18.86	0.12	0.58	-188.89	-25.93
04C171	37 30.11	114 54.85	4895.7	979463.45	-24.70	0.03	0.44	-192.62	-29.65
04C172	37 30.03	114 54.27	4851.1	979464.46	-27.76	0.01	0.42	-194.19	-31.16
04C173	37 29.94	114 53.63	4799.9	979467.08	-29.82	0.01	0.42	-194.49	-31.43
04C174	37 29.86	114 52.25	4775.7	979466.77	-32.29	0.03	0.51	-196.04	-32.95
04C175	37 29.70	114 51.31	4863.5	979460.68	-29.90	0.03	0.58	-196.58	-33.48
04C176	37 30.37	114 52.47	4783.1	979469.24	-29.87	0.03	0.49	-193.89	-30.42
04C177	37 31.32	114 52.05	4836.1	979466.89	-28.62	0.03	0.50	-194.45	-30.27
04C178	37 32.05	114 52.49	4821.1	979470.46	-27.52	0.02	0.44	-192.89	-28.20
04C179	37 31.62	114 51.08	4964.1	979458.69	-25.23	0.04	0.57	-195.37	-30.86
04C180	37 32.37	114 51.67	4912.3	979462.93	-26.95	0.04	0.49	-195.39	-30.40
04C181	37 32.93	114 50.73	5073.0	979454.48	-21.11	0.05	0.56	-194.99	-29.48
04C182	37 34.19	114 52.25	4869.2	979468.45	-28.13	0.02	0.38	-195.21	-29.02
04C183	37 34.98	114 52.98	4839.7	979472.43	-28.07	0.00	0.32	-194.20	-27.52
04C184	37 35.32	114 53.31	4863.3	979472.10	-26.68	0.01	0.30	-193.63	-26.76
04C185	37 35.73	114 53.66	4895.7	979471.44	-24.89	0.01	0.28	-192.98	-25.84
04C186	37 36.37	114 54.25	4961.4	979470.96	-20.13	0.02	0.28	-190.46	-23.04
04C187	37 37.20	114 45.07	5313.1	979468.89	9.65	0.39	1.20	-171.80	-2.80
04C188	37 36.03	114 41.69	6070.4	979414.11	27.75	0.61	1.80	-178.98	-10.45
04C189	37 34.29	114 48.37	5370.7	979442.36	-7.23	0.09	0.85	-190.99	-24.39
04C190	37 36.38	114 54.25	4966.0	979470.99	-19.68	0.02	0.28	-190.17	-22.75
04C191	37 54.74	114 51.85	4988.6	979509.56	-5.78	0.08	0.44	-176.89	1.71
04C192	37 55.06	114 52.30	5044.2	979504.69	-5.89	0.08	0.46	-178.88	-0.18
04C193	37 55.84	114 52.78	5164.1	979500.52	0.07	0.09	0.48	-177.00	2.08
04C194	37 56.18	114 53.18	5272.2	979494.06	3.28	0.22	0.63	-177.34	1.88
04C195	37 55.55	114 54.44	5281.4	979492.81	3.81	0.09	0.51	-177.24	1.45
04C196	37 55.63	114 53.90	5246.8	979495.29	2.92	0.17	0.59	-176.87	1.95
04C197	37 55.52	114 53.41	5199.1	979498.20	1.51	0.07	0.48	-176.76	2.05
04C198	37 54.83	114 52.50	5055.7	979503.58	-5.58	0.05	0.44	-178.98	-0.42
04C199	37 55.02	114 52.92	5100.7	979502.48	-2.73	0.05	0.47	-177.64	0.95

04C200	37 54.91	114 53.37	5176.3	979498.68	0.74	0.07	0.49	-176.74	1.73
04C201	37 53.67	114 52.26	4977.5	979510.79	-4.03	0.09	0.51	-174.68	3.23
04C202	37 53.47	114 53.80	5322.7	979486.84	4.76	0.45	1.00	-177.22	0.36
04C203	37 53.31	114 53.40	5226.8	979490.83	-0.03	0.44	0.94	-178.78	-1.23
04C204	37 52.92	114 52.84	5074.0	979500.13	-4.52	0.36	0.82	-178.17	-0.77
04C205	37 52.46	114 52.77	5035.4	979502.94	-4.67	0.45	0.91	-176.90	0.22
04C206	37 51.27	114 52.36	4929.4	979506.36	-9.47	0.07	0.49	-178.50	-1.96
04C207	37 51.29	114 50.94	4772.8	979510.46	-20.12	0.03	0.34	-183.94	-7.16
04C208	37 52.00	114 48.26	4617.8	979504.12	-42.07	0.00	0.25	-200.67	-23.10
04C209	37 51.93	114 49.59	4678.3	979517.33	-23.07	0.01	0.27	-183.73	-6.38
04C210	37 52.45	114 50.71	4751.7	979515.12	-19.14	0.02	0.35	-182.23	-4.74
04C211	37 49.29	114 50.67	4714.7	979511.69	-21.43	0.02	0.33	-183.27	-7.64
04C212	37 49.37	114 51.68	4831.5	979504.40	-17.86	0.04	0.40	-183.63	-8.14
04C213	37 36.38	114 54.25	4963.8	979470.98	-19.90	0.02	0.28	-190.31	-22.88

Table A2. Physical property measurements of rock samples collected in 2003 and 2004.

Station	Rock type	Grain density (g/cm^3)	Saturated bulk density (g/cm^3)	Dry bulk density (g/cm^3)	Porosity (%)	Susceptibility (10^{-3} SI)
03L002	Carbonate	2.71	2.70	2.69	0.7	0.02
03L003	Carbonate	2.67	2.67	2.67	0.2	0.03
03L004	Interm. Volcanic	2.64	2.62	2.62	0.8	12.00
03L005	Felsic Volcanic	2.44	2.41	2.40	1.8	3.83
03L009	Carbonate	2.70	2.70	2.69	0.3	0.01
03L010	Sandstone	2.42	2.37	2.34	3.6	0.03
03L038	Quartzite	2.64	2.62	2.61	1.1	0.03
03L039	Felsic Volcanic	2.56	2.52	2.49	3.1	0.04
03L012	Carbonate	2.82	2.79	2.77	1.7	0.02
03L013	Carbonate	2.66	2.59	2.55	4.0	0.01
03L014	Carbonate	2.68	2.64	2.62	2.3	0.02
03L016	Carbonate	2.70	2.69	2.69	0.3	0.01
03L017	Carbonate	2.70	2.69	2.68	0.7	0.02
03L018	Granite	2.51	2.49	2.47	1.4	0.15
03L019	Interm. Volcanic	2.43	2.41	2.40	1.4	0.27
03L020	Felsic Volcanic	2.55	2.51	2.48	2.9	5.32
03L021	Carbonate	2.69	2.64	2.62	2.7	0.04
03L034	Sandstone	2.62	2.59	2.57	1.9	0.03
03L037	Sandstone	2.60	2.59	2.59	0.7	0.02
03L023	Carbonate	2.84	2.83	2.83	0.4	0.01
03L024	Carbonate	2.84	2.81	2.79	1.5	0.02
03L025	Carbonate	2.85	2.82	2.81	1.2	0.01
03L026	Carbonate	2.80	2.77	2.75	1.7	0.01
03L027	Felsic Volcanic	2.24	2.14	2.05	9.4	1.84
03L028	Carbonate	2.64	2.60	2.57	2.6	0.05
03L029	Carbonate	2.66	2.64	2.62	1.5	0.03
03L030	Carbonate	2.70	2.68	2.67	0.8	0.02
03L031	Carbonate	2.68	2.66	2.64	1.4	0.01
03L032	Carbonate	2.69	2.66	2.65	1.5	0.02
03L033	Carbonate	2.85	2.84	2.83	0.7	0.00
03L040	Carbonate	2.70	2.69	2.68	0.7	0.03
03L041	Sandstone	2.56	2.53	2.51	1.8	0.03
03L043	Carbonate	2.69	2.66	2.64	2.1	0.02
03L044	Quartzite	2.64	2.63	2.63	0.3	0.04
03L045	Quartzite	2.61	2.60	2.59	0.5	0.04
03L046	Quartzite	2.65	2.65	2.64	0.5	0.06
03L048	Carbonate	2.70	2.68	2.67	1.1	0.03
03L049	Carbonate	2.70	2.69	2.69	0.3	0.02
03L050	Carbonate	2.85	2.84	2.84	0.6	0.02
03L051	Carbonate	2.81	2.78	2.76	1.8	0.02

03L052	Carbonate	2.68	2.61	2.57	4.0	0.01
03L053	Carbonate	2.70	2.69	2.69	0.7	0.27
03L054	Sandstone	2.60	2.58	2.56	1.9	0.02
03L055	Sandstone	2.56	2.48	2.43	5.4	0.05
03L057	Carbonate	2.85	2.85	2.85	0.2	0.03
03L058	Carbonate	2.68	2.67	2.66	0.8	0.02
03L059	Felsic Volcanic	2.59	2.52	2.48	4.5	8.53
03L060	Felsic Volcanic	2.61	2.57	2.54	2.8	12.40
03L061	Carbonate	2.70	2.69	2.69	0.4	0.01
03L062	Carbonate	2.84	2.84	2.83	0.3	0.03
03L063	Carbonate	2.86	2.86	2.85	0.2	0.02
03L064	Carbonate	2.67	2.62	2.59	3.3	0.01
03L065	Interm. Volcanic	2.36	2.32	2.29	2.9	7.43
04L015	Carbonate	2.71	2.70	2.69	0.8	0.02
04L020	Felsic Volcanic	2.06	1.73	1.43	44.7	0.88
04L021a	Felsic Volcanic	2.07	1.98	1.90	9.2	0.64
04L021b	Felsic Volcanic	2.50	2.46	2.43	2.9	6.34
04L023	Sandstone	2.47	2.37	2.30	7.2	0.71
04L053	Carbonate	2.72	2.71	2.71	0.7	0.03
04L062	Carbonate	2.73	2.72	2.71	0.6	0.03
04L097	Carbonate	2.74	2.72	2.72	0.8	0.04
04L098	Carbonate	2.72	2.70	2.69	1.3	0.03
04L100	Sandstone	2.65	2.64	2.64	0.5	0.13
04L101	Sandstone	2.64	2.62	2.61	1.0	0.02
04L114	Carbonate	2.70	2.68	2.67	1.0	0.05
04L120	Carbonate	2.85	2.84	2.83	0.6	0.03
04L125	Carbonate	2.76	2.74	2.72	1.2	0.02
04L127	Sandstone	2.66	2.61	2.58	3.1	0.12
04L128	Carbonate	2.70	2.67	2.66	1.2	0.04
04L137	Felsic Volcanic	2.51	2.32	2.19	14.6	5.91
04L147	Carbonate	2.69	2.66	2.65	1.7	0.02
04L171	Felsic Volcanic	2.48	2.38	2.31	7.2	4.56
04L138	Quartzite	2.60	2.59	2.59	0.7	0.00
04L174	Felsic Volcanic	2.41	2.29	2.21	9.2	1.57
04L177	Felsic Volcanic	2.52	2.39	2.30	9.5	5.07
04L186	Felsic Volcanic	2.58	2.54	2.51	3.0	8.15
04L188	Felsic Volcanic	2.59	2.55	2.52	2.8	16.90
04C013	Felsic Volcanic	2.41	2.22	2.09	15.2	0.10
04C025	Felsic Volcanic	2.60	2.58	2.57	1.3	8.14
04C026	Felsic Volcanic	2.39	2.32	2.28	4.8	2.72
04C028	Carbonate	2.85	2.84	2.84	0.4	0.02
04C029	Interm. Volcanic	2.57	2.52	2.49	3.1	11.40
04C030	Felsic Volcanic	2.61	2.56	2.53	3.4	7.37
04C031	Felsic Volcanic	2.53	2.43	2.36	7.4	0.71
04C032	Felsic Volcanic	2.57	2.54	2.52	2.0	2.43
04C033	Felsic Volcanic	2.60	2.45	2.36	10.1	0.12
04C034	Sandstone	2.63	2.61	2.60	0.9	0.06
04C035	Carbonate	2.70	2.64	2.60	3.7	0.01
04C036	Carbonate	2.81	2.80	2.79	0.8	0.01
04C037	Carbonate	2.75	2.74	2.73	1.1	0.02
04C038	Carbonate	2.83	2.82	2.81	0.8	0.01
04C039	Felsic Volcanic	2.58	2.46	2.39	7.7	4.77
04C040	Felsic Volcanic	2.53	2.40	2.32	8.9	0.36
04C041	Felsic Volcanic	2.47	2.27	2.13	15.9	0.35
04C057	Felsic Volcanic	2.45	2.35	2.28	7.2	0.84
04C058	Felsic Volcanic	2.49	2.32	2.21	12.7	0.27
04C059	Felsic Volcanic	2.40	2.28	2.20	8.8	1.25
04C060	Felsic Volcanic	2.42	2.25	2.13	13.5	5.94

04C061	Felsic Volcanic	2.34	2.27	2.22	5.5	1.42
04C062	Felsic Volcanic	2.46	2.23	2.08	18.4	0.18
04C063	Felsic Volcanic	2.44	2.23	2.08	17.4	2.00
04C064	Felsic Volcanic	2.41	2.33	2.27	6.4	2.09
04C042	Felsic Volcanic	2.45	2.18	1.99	23.1	1.16
04C043	Felsic Volcanic	2.52	2.43	2.36	6.4	0.30
04C044	Mafic Volcanic	2.28	2.11	1.97	16.2	1.44
04C045	Interm. Volcanic	2.55	2.48	2.43	4.9	0.34
04C046	Felsic Volcanic	2.43	2.30	2.22	9.6	0.75
04C049	Felsic Volcanic	2.47	2.33	2.24	10.4	0.20
04C050	Felsic Volcanic	2.49	2.34	2.24	10.9	0.27
04C051	Felsic Volcanic	2.47	2.29	2.17	13.6	0.11
04C052	Felsic Volcanic	2.43	2.38	2.34	3.6	0.45
04C053	Felsic Volcanic	2.45	2.32	2.23	10.0	0.21
04C054	Interm. Volcanic	2.40	2.36	2.34	2.6	1.31
04C066	Felsic Volcanic	2.35	2.27	2.21	6.5	2.58
04C067	Carbonate	2.45	2.34	2.26	8.2	0.70
04C068	Interm. Volcanic	2.36	2.33	2.31	1.8	0.92
04C069	Felsic Volcanic	2.52	2.43	2.37	6.6	6.41
04C070	Interm. Volcanic	2.68	2.66	2.64	1.6	12.40
04C071	Interm. Volcanic	2.78	2.75	2.74	1.5	14.70
04C072	Felsic Volcanic	2.40	2.09	1.87	28.8	0.52
04C073	Felsic Volcanic	2.20	2.09	1.99	10.5	1.37
04C074	Mafic Volcanic	2.69	2.65	2.63	2.2	8.89
04C075	Felsic Volcanic	2.47	2.44	2.43	1.7	3.90
04C076	Felsic Volcanic	2.22	2.08	1.96	13.3	2.74
04C077	Felsic Volcanic	2.44	2.25	2.13	14.9	2.29
04C078	Quartzite	2.57	2.55	2.54	1.4	0.03
04C079	Interm. Volcanic	2.66	2.64	2.63	1.1	8.30
04C080	Felsic Volcanic	2.54	2.51	2.49	2.2	8.25
04C081	Interm. Volcanic	2.56	2.49	2.45	4.5	4.11
04C082	Interm. Volcanic	2.61	2.58	2.57	1.8	2.48
04C083	Felsic Volcanic	2.59	2.58	2.57	1.0	14.20
04C084	Felsic Volcanic	2.75	2.73	2.72	1.2	9.00
04C085	Felsic Volcanic	2.32	2.20	2.11	10.2	1.55
04C086	Felsic Volcanic	2.31	1.95	1.67	38.5	0.69
04C087	Felsic Volcanic	2.45	2.28	2.15	14.0	3.09
04C089	Interm. Volcanic	2.66	2.66	2.65	0.5	13.40
04C090	Carbonate	2.85	2.84	2.83	0.5	0.01
04C091	Carbonate	2.81	2.77	2.75	2.0	0.03
04C092	Carbonate	2.39	2.28	2.20	8.8	0.00
04C093	Carbonate	2.61	2.49	2.41	8.1	0.03
04C094	Carbonate	2.79	2.76	2.74	1.8	0.00
04C095	Carbonate	2.67	2.61	2.58	3.5	0.05
04C096	Carbonate	2.63	2.58	2.56	2.8	0.01
04C097	Carbonate	2.76	2.73	2.71	1.6	0.02
04C108	Felsic Volcanic	2.43	2.30	2.22	9.5	1.68
04C109	Felsic Volcanic	2.40	2.25	2.14	12.3	0.26
04C163	Felsic Volcanic	2.46	2.35	2.28	8.2	6.00
04C176	Interm. Volcanic	2.17	2.16	2.15	0.8	0.47
04C194	Felsic Volcanic	2.57	2.53	2.51	2.1	5.79
04C196	Sandstone	2.63	2.62	2.62	0.5	0.13
04C200	Felsic Volcanic	2.47	2.35	2.26	9.6	1.21
04C202	Mafic Volcanic	2.53	2.52	2.51	0.6	5.36
04C203	Felsic Volcanic	2.34	2.20	2.09	11.8	0.37